

# Asymptotic Behavior of Excitable Cellular Automata

Richard Durrett and David Griffeath

## CONTENTS

- 1. Introduction
- 2. Proof of Theorems 1.2 and 1.3
- 3. Computer Horticulture
- 4. Prebug Upper Bounds
- 5. Prebug and Spiral Lower Bounds for  $p = 2$
- 6. Prebug and Spiral Lower Bounds for  $p = \infty$
- Acknowledgements
- Software Availability
- References

---

We study two families of excitable cellular automata known as the *Greenberg–Hastings model* and the *cyclic cellular automaton*. Each family consists of local deterministic oscillating lattice dynamics, with parallel discrete-time updating, parametrized by the range  $\rho$  of interaction,  $l^p$  shape of its neighbor set, threshold  $\theta$  for contact updating, and number  $\kappa$  of possible states per site. These models are mathematically tractable prototypes for the spatially distributed periodic wave activity of so-called excitable media observed in diverse disciplines of experimental science.

Fisch, Gravner and Griffeath [Fisch et al. 1991] studied experimentally the ergodic behavior of these models on  $\mathbf{Z}^2$ , started from random initial states. Among other phenomena, they noted the emergence of asymptotic phase diagrams (and dynamics on  $\mathbf{R}^2$ ) in the threshold-range scaling limit as  $\rho, \theta \rightarrow \infty$  with  $\theta/\rho^2$  constant.

Here we present several rigorous results and some experimental findings concerning various phase transitions in the asymptotic diagrams. Our efforts focus on evaluating  $\text{bend}(p)$ , the limiting threshold cutoff for existence of the spirals that characterize many excitable media. Our main results are formulated in terms of  $\text{spo}(p)$ , the cutoff for existence of *stable periodic objects* that arise as spiral cores. Some subtle consequences of anisotropic neighbor sets ( $p \neq 2$ ) are also discussed; the case of box neighborhoods ( $p = \infty$ ) is examined in detail.

---

## 1. INTRODUCTION

In the two-dimensional *Greenberg–Hastings model*, or GHM [Greenberg et al. 1978; Greenberg and Hastings 1978] we imagine the points of  $\mathbf{Z}^2$  as being occupied by neurons that can be rested (state 0), excited (state 1), or in a sequence of recovery states  $2, \dots, \kappa - 1$ , where  $\kappa \geq 3$ . The state of the system at time  $n$  is represented by a function  $\xi_n : \mathbf{Z}^2 \rightarrow \{0, 1, \dots, \kappa - 1\}$  that evolves according to the following simple rules:

AMS 1980 Subject Classification: Primary 60K35

This research was partially supported by research grants to each of the authors from the National Science Foundation.

- (a) If  $\xi_n(x) = i > 0$ , then  $\xi_{n+1}(x) = i + 1$ . (Note: throughout this paper arithmetic in the state space is done modulo  $\kappa$ .)
- (b) If  $\xi_n(x) = 0$  and at least  $\theta$  neighbors are 1, then  $\xi_{n+1}(x) = 1$ ; otherwise  $\xi_{n+1}(x) = 0$ .

Here the neighbors of  $x$  are the points  $y$  such that  $y - x \in N$  for some prescribed set  $N$ . For a given  $p \in [1, \infty)$ , we will always take for  $N$  the closed ball  $B_p(\rho)$  of radius  $\rho$  in the  $l^p$  metric:

$$N = \{y : \|y\|_p \leq \rho\},$$

where  $\|y\|_p = (|y_1|^p + |y_2|^p)^{1/p}$  for  $p < \infty$ , and  $\|y\|_\infty = \max\{|y_1|, |y_2|\}$ . We call  $\theta$  the *threshold* and  $\rho$  the *range*.

The state at  $x$  is said to update *automatically* in case (a), and *by contact* in case (b).

The closely related *cyclic cellular automaton*, or CCA [Fisch et al. 1991, 1992] evolves similarly, except that all sites update by contact (a site in state  $i$  updates when there are at least  $\theta$  neighbors in state  $i + 1$ ).

These two parametrized families of cellular automata are prototypes for *excitable media*: periodic wave dynamics that arise in many areas of applied science. In two dimensions such systems are typically characterized by the emergence of spatially distributed “target patterns” and/or spirals. One of the more bizarre real-world examples of an excitable medium is Cyclic AMP wave transmission in the “amoeba aggregation phase” of the slime mold *Dictyostelium discoideum*: see [Newell 1983] for a nice photograph of the characteristic wave patterns. (Later on this creature becomes a multicellular slug, but that’s another story!)

Beginning with the seminal work of Wiener and Rosenblueth [1946], and fueled by discovery of the Belousov–Zhabotinski oscillating chemical reaction in the late sixties (see [Winfree 1974]), a sizable body of knowledge has developed on the subject of excitable media. Over the past decade, in particular, rapid advances in computer technology have sparked an explosion of research activity. References [Gerhardt et al. 1990; Kapral 1991; Mar-

cus et al. 1991; Winfree 1987] are representative of recent experimental and applied modeling efforts, while [Durrett 1992; Durrett and Neuhauser 1991; Durrett and Steif 1991, 1993; Fisch et al. 1993; Gravner; Gravner and Griffeath 1994] contain the beginnings of a rigorous mathematical theory. See also [Dewdney 1988, 1989; Durrett 1993; Griffeath 1988; Mikhailov 1991; Toffoli and Margolus 1987] for expository accounts of excitable cellular automata, and [Muller et al. 1986] for pictures of actual Belousov–Zhabotinski spirals.

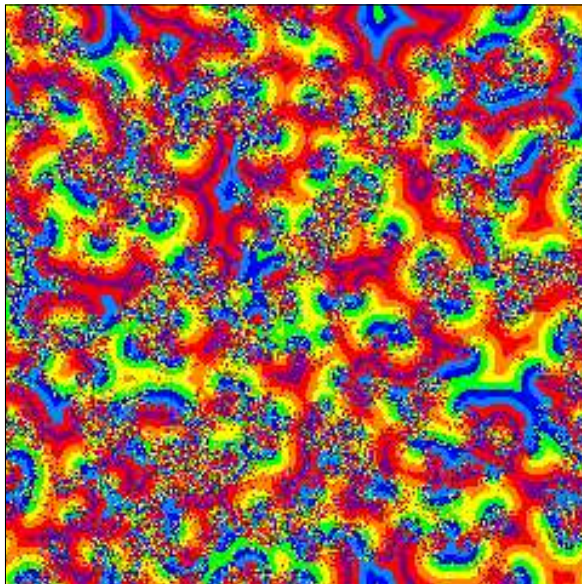
We should note that other paradigms such as partial differential equations and coupled lattice maps are also often used to model excitable systems. In this paper, however, we will focus on detailed aspects of GHM and CCA dynamics.

A primary tool for the analysis of excitable cellular automata is computer visualization, so we refer to the  $\kappa$  possible states at each site as *colors*. The reason for our interest in these systems and the motivation for much of this paper can be seen in Figure 1, which are representative snapshots of the GHM evolution on a  $240 \times 240$  grid with  $p = 2$ ,  $\rho = \sqrt{20}$ , and various values of  $\theta$  and  $\kappa$ . In the experiments depicted in this figure, as throughout most of the paper, we started from *primordial soup*, that is, the product measure with uniform density  $1/\kappa$ . Thus, the initial colors of sites are independent and take the  $\kappa$  possible values with equal probability.

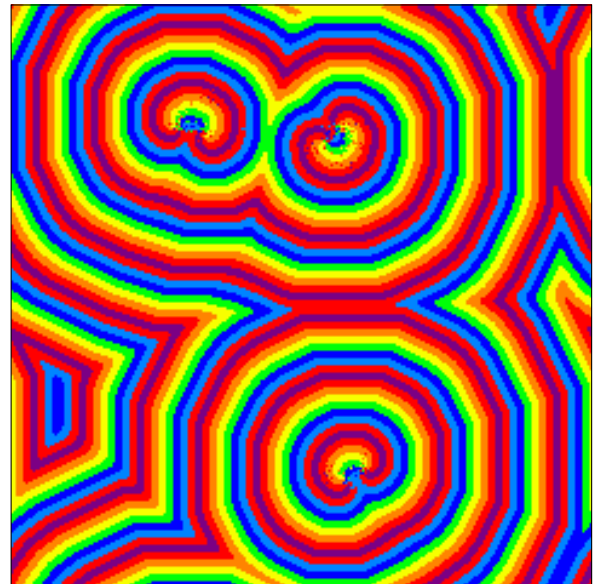
One should bracket the images in Figure 1 with two less interesting scenarios: when  $\theta = 5$  and  $\kappa = 6$  the image remains virtually indistinguishable from random noise, and when  $\theta = 11$  and  $\kappa = 5$  it evolves to the *trap*  $\xi(x) \equiv 0$  from which no changes are possible.

Evidently GHM can self-organize starting from primordial soup. Similar but even more exotic self-organization takes place in CCA; see [Fisch et al. 1991, color plates E–H] for some representative patterns.

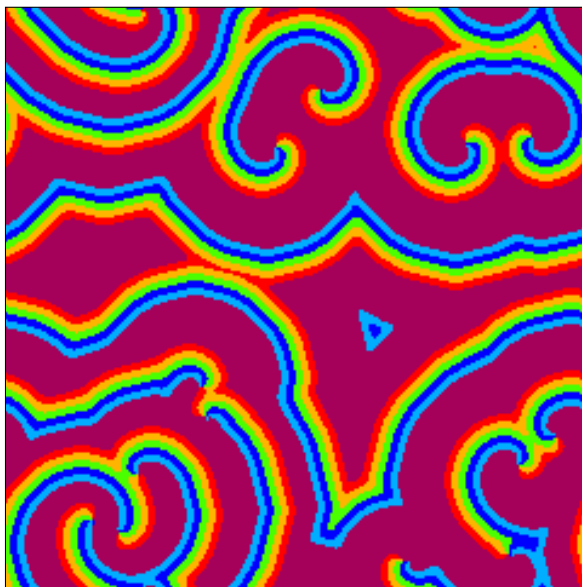
The basic problem concerning excitable cellular automata is the classification of their limiting behavior as  $n \rightarrow \infty$  (with probability one, on the



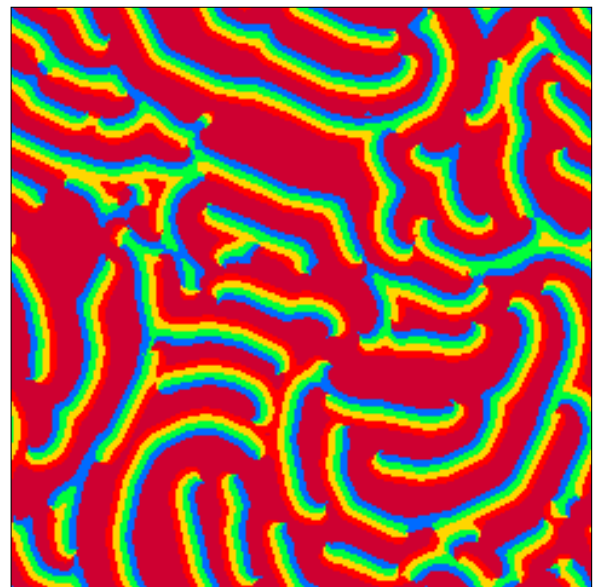
$\theta = 6, \kappa = 8$



$\theta = 7, \kappa = 8$



$\theta = 9, \kappa = 6$



$\theta = 10, \kappa = 5$

**FIGURE 1.** Representative snapshots of the evolution of the Greenberg–Hastings model on a  $240 \times 240$  grid with  $p = 2$ ,  $\rho = \sqrt{20}$ , and various values of  $\theta$  and  $\kappa$ . (The shape of  $N = B_p(\rho)$  is shown in the middle.) The initial states were created by random assignment of colors to each site with equal probability, and the snapshots were taken after 100 steps. Boundary conditions are periodic, that is, opposite edges are identified.

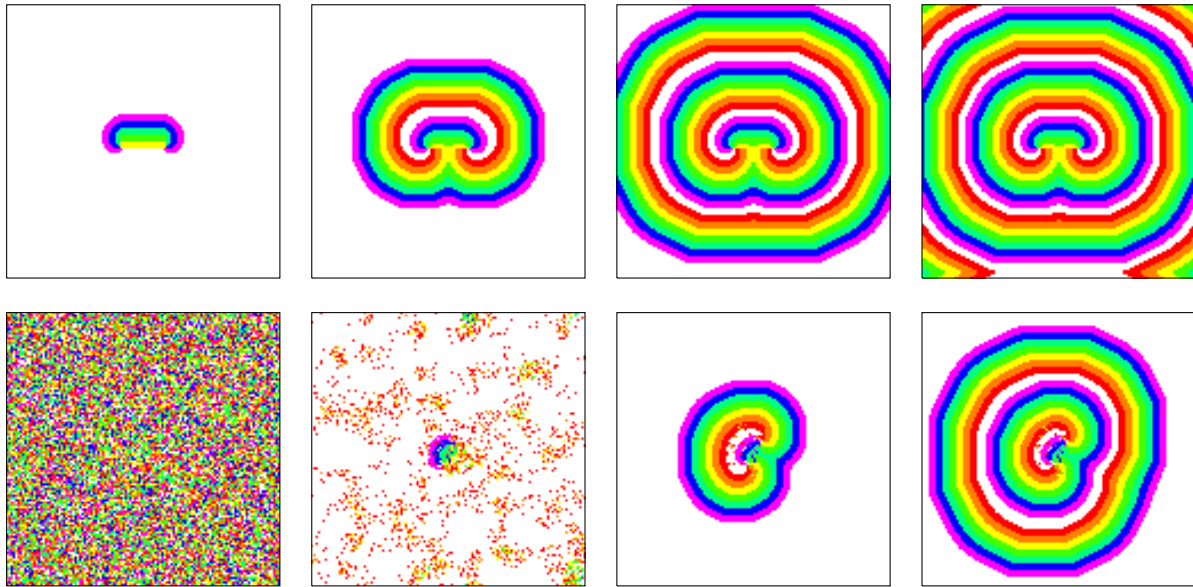


**FIGURE 2.** Greenberg–Hastings spirals from the band test (top) and nucleation (bottom). The parameters are  $p = 2$ ,  $\rho = \sqrt{20}$ ,  $\theta = 7$ ,  $\kappa = 8$ ; the dimensions of the band are  $l = 25$  and  $w = 2$ . Times are 3, 11, 19 and 27 for the top row and 0, 8, 16 and 24 for the bottom. Compare Figure 1 (top right).

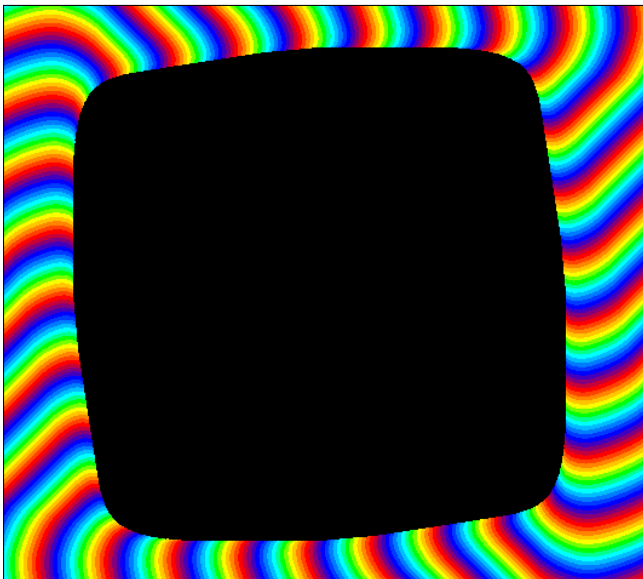


**FIGURE 3.** A spiral core spo for  $p = \infty$ ,  $\rho = 10$ ,  $\theta = 70$ . The 464 strands have been colored mod 16, so one can imagine  $\kappa = 16$ , but in fact any  $\kappa \geq 4$  will do as well; what matters is how a wave that is (barely) able to bend wraps around, in this case moving clockwise. The black area is irrelevant to the spo; nothing that happens there, or outside the picture, can disturb the behavior of the ring.

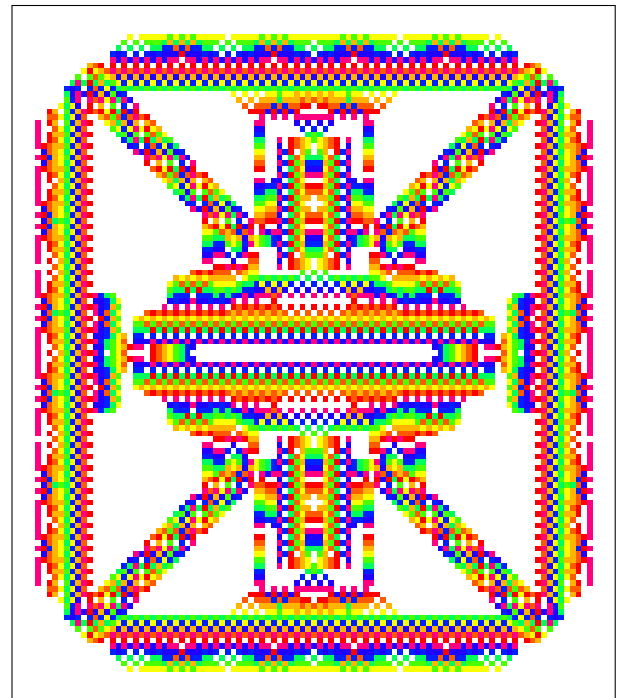


**FIGURE 4.** Smallest known ten-color spo with the parameters  $p = \infty$ ,  $\rho = 1$  and  $\theta = 2$ , due to D. Pritikin. The colors are as follows: white = 0, bright red = 1, then across the spectrum to violet-red.

infinite lattice) based on the values of  $p, \rho, \theta$  and  $\kappa$ . One possibility, for large thresholds  $\theta$ , is *fixation*: each site is eventually painted a final color. In GHM this amounts to global relaxation, or dying out:

$$\lim_{n \rightarrow \infty} \xi_n(x) = 0 \quad \text{for all } x.$$

CCA has an enormous set of traps since there is no automatic updating, so the final fixated state retains evidence of the original soup.

A more interesting outcome is *local periodicity with period  $\kappa$* : here,  $\xi_n$  does not fixate, but

$$\lim_{n \rightarrow \infty} \xi_{n\kappa}(x) = \xi_\infty(x) \quad \text{for all } x.$$

An argument from [Fisch et al. 1992] shows that:

**Theorem 1.1.** *For  $\theta = 1, \kappa \geq 3$ , and  $\rho \geq 1$ , any GHM or CCA system is locally periodic of period  $\kappa$ , with probability one.*

*Outline of proof.* Somewhere in the random initial state is a *clock*, that is, a loop of sites on which all  $\kappa$  colors are arranged cyclically (necessarily cycling more than once if  $\kappa$  is odd). Since  $\theta = 1$ , the color at every site of the clock advances each time, so the set of sites  $\mathcal{Z}$  that eventually change color every time is nonempty. To argue that  $\mathcal{Z} = \mathbf{Z}^2$ , suppose not and find  $x \notin \mathcal{Z}$  and  $y \in \mathcal{Z}$  that are neighbors. Since the value at  $x$  cannot continually cycle as rapidly as the value at  $y$ , it is easy to see that eventually we will have  $\xi_n(y) = \xi_n(x) + 1$ ; from then on  $x$  will be periodic with period  $\kappa$ , contradicting the choice of  $x$ .  $\square$

This proof incorporates the simplest example of a *stable periodic object*, or spo. By definition, an spo is a finite set  $A \subset \mathbf{Z}^2$  together with a mapping  $\zeta : A \rightarrow \{0, 1, \dots, \kappa - 1\}$ , such that, for each  $x \in A$ ,

$$|\{y \in A : y - x \in N \text{ and } \zeta(y) = \zeta(x) + 1\}| \geq \theta.$$

In words, each site  $x \in A$  sees at least  $\theta$  neighbors of the next color, and hence advances each time, independently of the states of sites in the complement of  $A$ . (We remark that this notion continues

to make sense and to play a key role in dimensions greater than two.)

Existence of spo's for a given rule guarantees their presence somewhere in the primordial soup, and therefore ensures that the process cannot fixate. The systems in the top row of Figure 1 have an easy time manufacturing spo's out of randomness; we invite the reader to guess some of their locations in the graphics. For higher thresholds, as in the systems in the second row, it is much less clear whether spo's can be formed dynamically, whether they even exist, and whether the infinite system is locally periodic.

Our first result shows that spo's are abundant when  $\theta/|N|$  is sufficiently small.

**Theorem 1.2.** *Suppose  $\lambda < \frac{1}{2}$  and  $\theta/|N| \leq \lambda/\kappa$ , and let  $\zeta$  be the restriction of the initial random state to  $A = B_2(K\rho)$ . Then there exists  $K_\lambda < \infty$  such that, if  $K \geq K_\lambda$ , the probability that  $\zeta$  is an spo tends to 1 as  $\rho \rightarrow \infty$ .*

This theorem is easy to prove. Let  $\lambda'$  be the midpoint of  $(\lambda, \frac{1}{2})$ . If  $K$  is large enough, then for large  $\rho$  each site in  $A$  has at least  $\lambda'|N|$  neighbors in  $A$  and the law of large numbers implies that with high probability each site will have at least  $(\lambda/\kappa)|N|$  neighbors in each state. Using elementary reasoning in the spirit of the proof of Theorem 1.1, we will show in Section 2 that sufficiently large spo's grow to “enslave” any remaining nonperiodic sites, thereby establishing local periodicity for the same parameter region.

**Theorem 1.3.** *Suppose  $\lambda < \frac{1}{2}$  and  $\theta/|N| \leq \lambda/\kappa$ . If  $\rho$  is large, the system is locally periodic of period  $\kappa$ , with probability one.*

This, too, will be proved in Section 2.

When Theorems 1.2 and 1.3 apply, the threshold is sufficiently low that contact updating predominates from the beginning and little self-organization need take place. The case  $p = 2, \rho = \sqrt{20}, \theta = 5$ , and  $\kappa = 6$ , mentioned in connection with Figure 1, is typical of this “debris phase.” For intermediate thresholds, excitation is sustained only

in widely separated “nucleating centers,” but these locations are able to create spo’s that proceed to enslave their environment. In general, we suspect that the existence of an spo implies that the system becomes locally periodic with period  $\kappa$ . For instance, the systems corresponding to Figure 1 all have spo’s, and we believe they are all locally periodic. A proof of this conjecture would need to address various subtle distinctions. GHM rules, for instance, can produce stable patches of “all 0’s” mixed with stable patches of period  $\kappa$ . One example is the periodic core surrounding the hole in Figure 3 below.

To avoid such difficulties, we will concentrate here on the problem of existence of spo’s, and in particular on asymptotic results for the quantity  $\text{spo}_\kappa(\rho, p)$ , defined as the supremum of the values of  $\theta$  such that there exists an spo for  $N = B_p(\rho)$ . Our first step is to show that:

**Theorem 1.4.** *For any  $\kappa \geq 3$  and any  $p$ , the limit*

$$\text{spo}_\kappa(p) := \lim_{\rho \rightarrow \infty} \frac{\text{spo}_\kappa(\rho, p)}{\rho^2}$$

*exists.*

*Proof.* This follows from a soft “renormalization” argument that is simple enough to give in this introduction. By replacing each site in an spo with an  $m \times m$  square of the same color, it is easy to see ( $p = 1$  is the worst case) that

$$\text{spo}_\kappa((r + 2)m, p) \geq m^2 \text{spo}_\kappa(r, p). \tag{1.1}$$

Taking  $m = \lceil \rho / (r + 2) \rceil$  and using the fact that  $\text{spo}_\kappa(p, \rho)$  increases with  $\rho$ , we have

$$\begin{aligned} \liminf_{\rho \rightarrow \infty} \frac{\text{spo}_\kappa(\rho, p)}{\rho^2} &\geq \sup_r \frac{\text{spo}_\kappa(r, p)}{(r + 2)^2} \\ &\geq \limsup_{\rho \rightarrow \infty} \frac{\text{spo}_\kappa(\rho, p)}{\rho^2}. \quad \square \end{aligned}$$

Theorem 1.2 shows that  $\text{spo}_\kappa(p) > C_p / \kappa$  for some  $C_p$  not depending on  $\kappa$ . To see that  $\text{spo}_\kappa(p) \geq \frac{1}{8}$ , let  $r = \lceil (\rho + 1) / 2 \rceil$ , define squares

$$\begin{aligned} A_i &= [ir, (i + 1)r) \times [0, r), \\ B_i &= [(\kappa - i - 1)r, (\kappa - i)r) \times [r, 2r) \end{aligned}$$

for  $i = 0, \dots, \kappa - 1$ , and set  $\zeta(x) = i$  for  $x \in A_i \cup B_i$ . We leave it as an exercise for the reader to improve the bound  $\text{spo}_\kappa(p) \geq \frac{1}{8}$  for specific values of  $p$  and  $\kappa$  by using other shapes instead of squares. Some conjectures about the dependence of  $\text{spo}_\kappa(p)$  on  $\kappa$  will appear later in this Introduction. In general we expect that  $\text{spo}_\kappa(\rho, p)$  is a nonincreasing function of  $\kappa$ , but the only thing that is clear is that if  $k$  divides  $l$  then  $\text{spo}_k(\rho, p) \geq \text{spo}_l(\rho, p)$  since one can paint the  $l$ -color spo modulo  $k$ .

To try to compute  $\text{spo}_\kappa(\rho, p)$ , we will refine various experiments introduced by Fisch, Gravner, and Griffeath in [Fisch et al. 1991] (hereafter abbreviated [FGG]). The first is the *band test*, which refers to starting an excitable cellular automaton with 1’s on  $[-l, l] \times [0, w)$ , 2’s on  $[-l, l] \times [-w, 0)$ , and 0’s at all other sites. We call  $w$  the *width* and  $l$  the *length* of the band. The reason for interest in the band test can be seen in Figure 2, which gives the outcome when  $p = 2$ ,  $\rho = \sqrt{20}$ ,  $\theta = 7$ , and  $\kappa = 8$ . As indicated by the top row of snapshots, the excited region wraps in on itself and makes a spiral pair. These artificially produced spirals are similar to the ones generated by the same parameter values in Figure 1 (top right), but have neater centers. The similarity is far from accidental: the bottom row of Figure 2 details an instance of spiral formation starting from primordial soup. Note that a band is formed first, which then grows into a spiral pair.

Given  $\rho$  and  $p$ , [FFG] defines a critical value  $\text{bend}(\rho, p)$  as the smallest integer such that, for  $\theta > \text{bend}(\rho, p)$ , the band is unable to fold in on itself completely when  $\kappa \geq 4$  (we exclude the case  $\kappa = 3$  because it presents certain complications that we won’t go into). To illustrate this somewhat imprecisely defined notion we offer Figures 3

and 5, which describe affairs when  $p = \infty$ ,  $\rho = 10$ , and  $\theta = 70$  or  $71$ , respectively. For  $\theta = 70$  a judiciously designed GHM band test barely manages to form the stable spiral core pictured in Figure 3; the diameter of its hole is more than 900 cells. A ring around this hole of suitable shape and size constitutes an spo. For  $\theta = 71$ , on the other hand, the band test remains confined to the upper half-plane for all time; its ends stabilize as images under  $\pm 90^\circ$  rotations of the *bug* of constant width shown in Figure 5. This bug reproduces exactly, neither growing nor shrinking as it advances. We have not been able to make a spiral core when  $\theta = 71$ , so we conclude that  $\text{bend}(10, \infty) = 70$ .

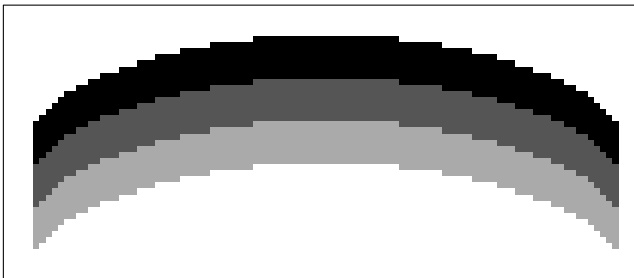


**FIGURE 5.** A bug of constant width for  $p = \infty$ ,  $\rho = 10$ ,  $\theta = 71$ .

On the basis of such experiments, it was conjectured in [FGG] that “if a wavefront can bend in on itself then the rule has spo’s.” Although we cannot prove this claim we have verified it in a great many cases, for various values of  $p$ . For instance, we have constructed spiral cores for the last two rules of Figure 1 by means of a variant of the band test that will be described in Section 3. In view of the large size of these synthetic cores, it is easy to understand why they fail to emerge from spatially homogeneous product measure in computer simulations.

[FGG] computed  $\text{bend}(\rho, p)$  for  $p = 1$  and  $p = \infty$ , and for  $1 \leq \rho \leq 6$ . Values for  $p = \infty$  and  $1 \leq \rho \leq 10$  are given in Table 1.

In all cases we have succeeded in constructing spo’s with  $\kappa = 4$  when  $\theta = \text{bend}(\rho, \infty)$ . A simple

$\rho$	$\text{bend}(\rho, \infty)$	$\frac{\text{bend}(\rho, \infty)}{\rho^2}$	$\text{bug}(\rho, \infty)$	$\frac{\text{bug}(\rho, \infty)}{\rho^2}$
1	1	1.000	2	2.000
2	4	1.000	4	1.000
3	7	.777	8	.889
4	12	.750	13	.813
5	18	.720	20	.800
6	26	.722	28	.778
7	35	.714	38	.776
8	45	.703	48	.750
9	57	.703	60	.741
10	70	.700	74	.740

**TABLE 1.** Values of  $\text{bend}(\rho, p)$  and  $\text{bug}(\rho, p)$  for  $p = \infty$  and  $1 \leq \rho \leq 10$ .

sharpening of inequality (1.1) for the the case  $p = \infty$  yields

$$\text{spo}_\kappa((\rho + 1)m, \infty) \geq m^2 \text{spo}_\kappa(\rho, \infty). \tag{1.2}$$

Using our spo for  $\rho = 10$ , we get

$$\text{spo}_4(\infty) \geq \frac{70}{121} \geq .578.$$

This “horticultural” approach to lower bounds for  $\text{spo}_\kappa(p)$  will be discussed at greater length in Section 3.

As motivation for the next development, we return to the case  $p = \infty$ ,  $\rho = 10$ ,  $\theta = 71$ . Recall that the excitation generated by a standard band test remains confined to an upper half-space, spreading out like a  $180^\circ$  cone with invariant ends that are  $\pm 90^\circ$  rotations of the form shown in Figure 5. If we surgically remove such an end and use it as the initial configuration for a modified band test, our little bug simply crawls upwards. Consequently the wave activity will never die out. Following [FGG], we let  $\text{bug}(\rho, p)$  be the largest threshold for which the band test can generate a wavefront that lives forever. Values of  $\text{bug}(\rho, \infty)$  for  $p = \infty$  and  $1 \leq \rho \leq 10$  are likewise given in Table 1.

It is natural to conjecture that

$$\text{bug}(p) := \lim_{\rho \rightarrow \infty} \frac{\text{bug}(\rho, p)}{\rho^2}$$

exists. Although the simple scaling argument for Theorem 1.4 does not apply directly, we will now introduce quantities that enable us to conjecture a precise value for  $\text{bug}(p)$  and to derive rigorous bounds. We think our methods strongly suggest that

$$\liminf_{\rho \rightarrow \infty} \frac{\text{bug}(\rho, p)}{\rho^2} \geq \limsup_{\rho \rightarrow \infty} \frac{\text{bend}(\rho, p)}{\rho^2},$$

with equality only in the isotropic case  $p = 2$ . As a consequence, for anisotropic neighbor sets the regime of excitable cellular automata between  $\text{bend}(\rho, p)$  and  $\text{bug}(\rho, p)$ , as described in [FGG], constitutes a bona fide phase in the threshold-range scaling limit rather than a boundary effect.

The main course of our investigation begins by letting  $\rho \rightarrow \infty$  with  $\theta = \theta_\infty \rho^2$  in order to obtain a limiting process on  $\mathbf{R}^2$  (compare [FGG, § 9]). A precise description of the limit will be given in Section 4, but in essence the continuum dynamics consist of truly massive parallel updating. Each site  $x$  in the plane has a color  $i$ ; in order to update by contact, the area of overlap between the Euclidean neighborhood of  $x$  and the region painted with color  $i + 1$  must exceed  $\theta$ . Our agenda is to study certain invariant and “superinvariant” wave fragments in this Euclidean setting.

Given continuous functions  $f(x) < g(x)$  on the interval  $(-l, r)$ , write

$$E = \{(x, y) : x \in (-l, r) \text{ and } f(x) < y < g(x)\}.$$

We fix our attention on the direction  $\alpha = \pi/2$  (“up”), and say that the region  $E$  is a *bug of length  $l + r$  and translation  $w$*  if, when we start with 1’s on  $E$  and 2’s on  $(0, -w) + E$ , the excited region at time 1 coincides with  $(0, w) + E$ . (Here  $z + E$  denotes the set  $E$  translated by  $z$ .) Note that if the shape of the excited region has stabilized, and moves up, its width should be constant and equal to  $w$  away from the ends; otherwise different parts of the bug would propagate at different speeds and the shape would not be maintained. The lattice bug in Figure 5 has constant width from one end to the other, but it is not hard to see that invariant

bugs on  $\mathbf{R}^2$  must have “rounded” ends. A *prebug of length  $l + r$  and translation  $w$*  is defined similarly, except that the excitation at time 1 should cover at least  $(0, w) + E$ .

Bugs and prebugs can be defined in an analogous way for other directions. Let  $\text{prebug}(\alpha, p)$  be the largest value of  $\theta$  for which a prebug exists in direction  $\alpha$ . Of course,  $\text{prebug}(\alpha, 2)$  is independent of  $\alpha$ . This case is particularly appealing to applied researchers because the limiting dynamics are isotropic (compare [Marcus et al. 1991]). In order to explore the effects of anisotropy we also focus on the case of box neighborhoods, that is,  $p = \infty$ . While the direction  $\alpha = \pi/2$  best matches the conventional representation of our prebug envelope functions  $f$  and  $g$ , the box symmetries imply that  $\text{prebug}(\cdot, \infty)$  has period  $\pi/2$  and is symmetric about  $\pi/4$ . Thus we choose  $[0, \pi/4]$  as the fundamental domain in this case. In Sections 4–6 we will prove the following bounds:

$$.6339 \leq \text{prebug}(0, \infty) \leq \frac{2}{3}; \tag{1.3}$$

$$.6355 \leq \text{prebug}(\pi/4, \infty) \leq \frac{80}{121} \leq .6612; \tag{1.4}$$

$$.5199 \leq \text{prebug}(\alpha, 2) \leq .5335. \tag{1.5}$$

The next result should explain our interest in the existence of prebugs.

**Theorem 1.5.** *For all  $\kappa \geq 3$ ,*

$$\text{spo}_\kappa(p) \geq \inf_\alpha \text{prebug}(\alpha, p). \tag{1.6}$$

*In particular,*

$$\text{spo}_\kappa(2) \geq .5199, \tag{1.7}$$

*and*

$$\text{spo}_\kappa(\infty) \geq .6123. \tag{1.8}$$

Inequality (1.7) is proved by taking the prebug that yields the lower bound in (1.5), shaving off a little bit, and arranging rotations of the prebug to produce an spo. The proofs of (1.6) and (1.8) are similar but more tedious: in anisotropic cases ( $p \neq 2$ ) one must produce a continuous family of prebugs,

one for each direction  $\alpha$ . Inequality (1.8) is worse than our lower bound in (1.3) and (1.4) since we have trouble constructing prebugs for  $\alpha$  near  $.21\pi$ , but we believe this is a technical shortcoming of our method. The spiral core in Figure 3 is apparently made up of a large collection of “viable ends” (ends that can advance without shrinking, similar to the bug ends with slightly higher threshold), so the picture at least suggests the following conjecture:

**Conjecture 1.6.** *There exists  $\kappa_0$  such that*

$$\text{spo}_\kappa(p) = \inf_\alpha \text{prebug}(\alpha, p). \quad (1.9)$$

for all  $\kappa \geq \kappa_0$ .

Equation (1.9) is false for  $\kappa = 3$ : Theorem 1.3 implies that

$$\lim_{\rho \rightarrow \infty} \frac{\text{spo}_3(\rho, \infty)}{\rho^2} \geq \frac{2}{3},$$

and we can in fact show that  $\text{spo}_3(\infty) > \frac{2}{3}$ . In keeping with [FGG], we believe that

$$\text{spo}_4(\rho, \infty) = \text{bug}(\infty),$$

and that  $\kappa_0 = 5$  in Conjecture 1.6. There is a lot of experimental evidence in support of these conclusions but we will not go into the details here.

We have equal faith in this conjecture:

**Conjecture 1.7.** *For every  $p$ ,*

$$\text{bug}(p) = \sup_\alpha \text{prebug}(\alpha, p). \quad (1.10)$$

Moreover, based on experiments that will be discussed in Section 3, we believe that the inf in (1.9) is attained at  $\alpha = \pi/4$ , while the sup in (1.10) is attained at  $\alpha = 0$ .

The methods of this paper provide a good deal of information about the existence of spirals. However, rigorous upper bounds on  $\text{spo}_\kappa(\rho, p)$  seem much more difficult to prove. How does one rule out the existence of spo’s with architectures altogether different from those produced by the band test? This issue is still quite murky even for the

so-called Moore neighborhood ( $p = \infty, \rho = 1$ ); perhaps the simplest open question is this:

**Problem 1.8.** *Show that if  $p = \infty$  and  $\rho = 1$ , spo’s do not exist for  $\theta = 3$ , or even  $\theta = 4$ .*

A proof in [Fisch et al. 1993] can be used to show nonexistence when  $\theta = 5$ . Of course any clock is an spo if  $\theta = 1$ . But already for  $\theta = 2$  it becomes quite challenging to find spo’s as  $\kappa$  increases. We leave it as an exercise for the reader to construct spo’s when  $\theta = 2$  and  $\kappa = 3$  or  $\kappa = 4$ ; one way is to run the GHM on a  $100 \times 100$  array, say, and capture an organizing center (compare [FGG, color plate C]). If  $\theta = 2$  and  $\kappa \geq 5$ , however, for any technologically feasible array the GHM dies out and CCA fixates starting from primordial soup. It is tempting to conclude that spo’s do not exist for these parameter values. Gradually over the past two years, in an impressive display of combinatorial creativity, D. Pritikin (private communication) has constructed increasingly complex spo’s for larger and larger numbers of colors. Figure 4 on page 186 shows the current record holder: the smallest known spo with  $\kappa = 10$  (its dimensions are approximately  $95 \times 111$  cells). Thus, a second open question, easy to state if not to solve, is this:

**Problem 1.9.** *For  $p = \infty, \rho = 1$ , and  $\theta = 2$ , find the supremum of all  $\kappa$  for which an spo exists.*

We believe this supremum is finite; in other words, spo’s do not exist once the number of colors is large.

Our intuition tells us that for  $\kappa$  large and  $\theta$  just below  $\text{bend}(\rho)$ , any alternative to the ring architecture of spiral cores should be less capable of making an spo. Thus we believe that Pritikin’s discoveries above  $\text{bend}(1)$  are artifacts of small range. But rigorous confirmation of this hunch remains one of the outstanding problems in the analysis of the phase diagrams for GHM and CCA rules.

The remainder of our paper is organized as follows. Theorems 1.2 and 1.3 are proved in Section 2. In Section 3 we describe a variety of computer experiments that shed light on asymptotic features

of GHM and CCA rules, with emphasis on the box neighborhood ( $p = \infty$ ). We describe the method used to construct the spo of Figure 3 and even larger spiral cores. We introduce additional cut-offs  $\text{end}_+(\alpha, \infty)$  and  $\text{end}_-(\alpha, \infty)$ , and explain their connection with  $\text{prebug}(\alpha, \infty)$ . We present tentative numerical estimation of the asymptotics for  $\text{bend}(\rho, \infty)$  and  $\text{bug}(\rho, \infty)$  by extrapolating from data for  $\rho \leq 40$ . Altogether, the findings of Section 3 depict a reasonably coherent and plausible scenario for a phase (with  $\theta/\rho^2$  between  $\text{spo}(p)$  and  $\text{bug}(p)$ ) in which there are no stable spiral cores and yet wave fragments propagate in certain directions.

The final three sections of the paper are devoted to rigorous results. In Section 4 we prove our upper bounds on  $\text{prebug}(\alpha, p)$ . Lower bounds on  $\text{prebug}(\alpha, 2)$  are proved in Section 5, and on  $\text{prebug}(\alpha, \infty)$  in Section 6.

**2. PROOFS OF THEOREMS 1.2 AND 1.3**

In this section we prove that the low-threshold regime  $\theta < |N|/2\kappa$  of parameter space is locally periodic in the threshold-range scaling limit. In fact, our method applies in any dimension  $d$  to show that essentially no self-organization takes place in this “debris-dominated” region. The first ingredient is a special case of [Durrett 1992, Lemma 2.1] or of the left-hand inequality in [Gravner and Griffeath 1994, (5.4)]; see also [Durrett 1993] for details of the proof.

**Lemma 2.1.** *Suppose  $b < \frac{1}{2}$ . There are constants  $\rho_0$  and  $r_0$  such that, if  $\rho \geq \rho_0$  and  $r \geq r_0$ , each site  $x \in B_2(r\rho)$  satisfies*

$$|(x + N) \cap B_2(r\rho)| \geq b|N|.$$

This simply expresses the geometric fact that the boundary of a large ball is locally flat.

The second ingredient in the proof of Theorem 1.2 is a standard large-deviations result. See, for example, [Durrett 1991, Chapter 1, §9].

**Lemma 2.2.** *Let  $X_1, X_2, \dots$  be independent, identically distributed Bernoulli random variables with  $P(X_i = 1) = \kappa^{-1}$  and  $P(X_i = 0) = 1 - \kappa^{-1}$ . Let  $S_n = X_1 + \dots + X_n$ . If  $a < \kappa^{-1}$ , there is a constant  $\gamma > 0$  such that*

$$P(S_n < an) \leq e^{-\gamma n}.$$

Theorem 1.2 is an easy consequence of the two lemmas. Theorem 1.3 is proved by starting from an spo in the initial soup and applying Lemma 2.1 to find a growing ball of periodic sites.

*Proof of Theorem 1.2.* Let  $b \in (\lambda, \frac{1}{2})$  and choose  $R \geq r_0$ , where  $r_0$  is as in Lemma 2.1. Pick  $a < \kappa^{-1}$  so that  $ab \geq \lambda\kappa^{-1}$ . If  $x \in A = B_2(R\rho)$  and  $\rho \geq \rho_0$ , Lemma 2.1 guarantees that  $x$  has at least  $n = b|N|$  neighbors in  $A$ . So Lemma 2.2 implies that, for any  $x \in A$ ,

$$|\{y \in A : y - x \in N, \xi_0(y) = \xi_0(x) + 1\}| \geq an \geq \theta$$

with probability at least  $1 - e^{-\gamma n}$ . Since  $|A| \leq C\rho^2$  and  $n \geq \delta\rho^2$ , summing the error probabilities we see that the probability that  $A$  is not an spo is at most  $|A|e^{-\gamma n}$ , which tends to 0 as  $\rho \rightarrow \infty$ , as claimed.  $\square$

*Proof of Theorem 1.3.* Let  $b = \lambda$  and pick  $r \geq r_0$ . For  $z \in \mathbf{Z}^2$ , let  $A_z$  be the event that the restriction of the initial random state to  $B_2(3r\rho z, r\rho)$  is an spo. For  $\rho$  sufficiently large, Theorem 1.2 evidently implies that  $P(A_z) > 0$ . Since the  $A_z$  are independent, the probability that  $A_z$  occurs for some  $z$  is 1. Pick, by any recipe, a  $z_0$  so that  $A_{z_0}$  occurs. Let  $B_t$  be the set of sites that fail to advance at some time  $s > t$ , and let  $x$  be any point in  $B_t$  with minimum distance from  $z_0$ . Lemma 2.1 implies that  $x$  has at least  $b|N|$  neighbors in the complement of  $B_t$ , and so has a set  $C_x$  of periodic neighbors that are all the same color, with  $|C_x| \geq b|N|/\kappa$ . Repeating the reasoning from the proof of Theorem 1.1, if we suppose that  $x \in B_s$  for all  $s > t$  then at some time  $r$  we must have  $\xi_r(x) = 0$  and  $\xi_r(y) = 1$  for all  $y \in C_x$ . Hence  $x \notin B_r$ , a contradiction which implies that  $B_t \downarrow \emptyset$  as  $t \rightarrow \infty$ .  $\square$

Theorems 1.2 and 1.3 are counterparts to results in [Durrett 1992] for multicolor interacting particle systems with large threshold and range. Although that paper deals with random dynamics, the regime corresponding to  $\{\theta < |N|/2\kappa\}$  is characterized by a fine-grained, asymptotically independent stochastic equilibrium. This is but one indication of the close connection between locally periodic cellular automata and oscillating Markovian lattice interactions such as the cyclic particle system [Griffeath 1988] and the epidemic with regrowth [Durrett and Neuhauser 1991]. Indeed, we expect that many qualitative features of the phase diagrams that are described in [FGG] are shared by their stochastic counterparts in [Durrett 1992] and elsewhere. Monte Carlo simulations on large arrays argue persuasively that excitable cellular automata are remarkably robust under random perturbations of the transition mechanism. One of our primary motivations for this and related work is the hope that in-depth analysis of GHM and CCA rules may ultimately shed light on the stochastic spatial modeling of phenomena such as epidemics and ecological competition.

### 3. COMPUTER HORTICULTURE

We now discuss various computer experiments that illuminate basic aspects of GHM/CCA dynamics. Readers who want to see at first hand the process of self-organization that leads to configurations such as those depicted in Section 1 can use the program Excite! [Fisch and Griffeath 1991] (see the section on software availability at the end of this paper).

First, we describe an efficient scheme for the generation of spo's that arise as spiral cores in excitable cellular automata. Starting from a band test with suitable length, width, and number of colors  $\kappa$ , [FGG] reported that a stable core typically forms dynamically, provided only that  $\theta \leq \text{bend}(\rho)$ . For thresholds close to the cutoff, though, the time until the system locks into a periodic configuration is often quite long due to interference between the two halves of a spiral pair or inter-

ference of a single spiral with itself. By slightly modifying the algorithm one can grow spo's with surprising reliability and efficiency.

For concreteness, we describe our method in the case  $p = \infty$ ,  $\rho = 10$ ,  $\theta = 70$  that produced Figure 3. We run our system on a square array of side 1100, with open boundary conditions. That is, we imagine that no other sites of  $\mathbf{Z}^2$  can become excited. Imitating a band test, we start by generating the four-color model with

$$\xi_0(x) = \begin{cases} 1 & \text{on } [0, 599] \times [50, 149], \\ 2 & \text{on } [0, 599] \times [150, 249], \\ 0 & \text{otherwise.} \end{cases}$$

To reduce interference and grow larger spo's, we place the band against the edge of the box instead of in the middle. Thus we get one spiral instead of a pair.

In the first phase of the procedure we run the system and only write newly excited sites to the screen, painting them a color equal to the time mod 16 so that we can watch how the front develops. In the particular case under consideration the excited region at time 928 coincides exactly with the excited region drawn at time 464, so we stop the evolution and change the number of colors from 16 to 464. In the second phase of the computation we paint the actual state of the process to the screen. After 464 time units the screen has become filled with colored strips and we obtain a large spo. One can, of course, have the computer check periodicity.

This strategy yields lower bounds for  $\text{spo}(\infty)$  via (1.2). The best result we have obtained using our  $2\text{K} \times 2\text{K}$  visualization technology is an spo with  $\rho = 36$  and  $\theta = 831$ , for a bound of

$$\text{spo}_4(\infty) \geq .607.$$

Since our "high school geometry" approach in Section 6 gives the better result (1.8), we will not describe the details of this experiment. Horticultural spo production can clearly be pushed further to produce much more accurate lower estimates on  $\text{spo}_\kappa(\infty)$  than (1.8), but we should point

out some interesting methodological challenges. As  $\rho$  increases, for  $\theta$  just below  $\text{bend}(\rho)$ , the size of the hole in a spiral core grows rapidly. It should not be necessary to store this hole in computer memory since almost none of it enters into the computation of a wave end's trajectory. A clever data structure should therefore be able to drastically reduce the amount of memory required. This would allow for much more accurate estimation of the cutoff. But the trajectory of an end becomes increasingly sensitive to boundary conditions, so great care must be taken to provide a wide enough boundary layer; otherwise the wavefront destabilizes and flies off the map. Needless to say, visualization is a very helpful tool in designing gigantic spo's.

The dynamics of large-range experiments such as those we have just described may be viewed as Riemann approximations to the limiting Euclidean dynamics mentioned in the Introduction. So insight into the relationship between limiting cutoffs  $\text{bend}$  and  $\text{bug}$  is also gained by observing the behavior of the band test for  $\text{bend}(\rho) \leq \theta \leq \text{bug}(\rho)$  when  $\rho$  is large. For the remainder of this section, let us discuss the regime  $\text{bend} \leq \theta \leq \text{bug}$  in the case  $p = \infty$ .

Figure 6 shows the trajectories of ends in modified band tests over this interval of thresholds when  $\rho = 12$ . The same qualitative behavior is observed in all the systems we have observed up to  $\rho = 40$ . Each shaded region represents the trace of excitation starting from a band shaped like a circular arc; such a shape leads the wavefront more efficiently toward its preferred geometry at the ends. The upper left picture has  $\theta = \text{bend}$ : the end traces out a corner of the large spo that it will eventually generate. Raising  $\theta$  by 1 we get the upper right trajectory: there is an angle (with the horizontal axis) somewhat less than  $45^\circ$  beyond which the end is unable to bend. A yet higher threshold produces the trace on the lower left: a stable cone of excitation spreads out with an opening of less than  $90^\circ$ . Finally, at the lower right, once  $\theta$  exceeds  $\text{bug}$  the excitation withers away from its ends.

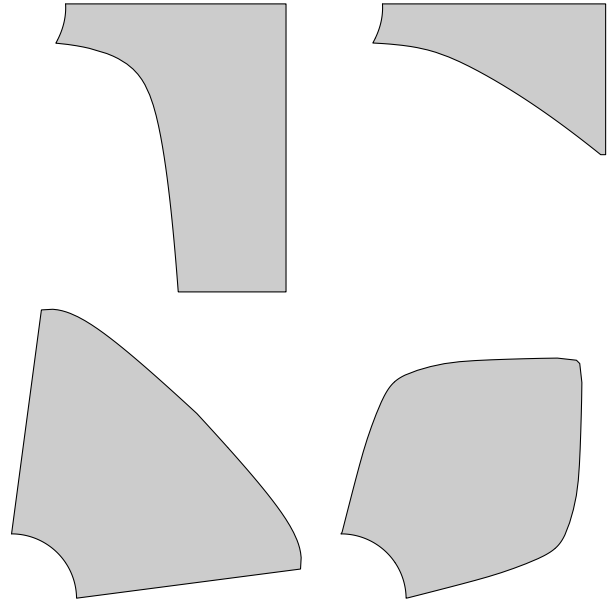


**FIGURE 6.** Trace of the excited region for  $p = \infty$ ,  $\rho = 12$  and increasing values of  $\theta$ . (The scale is about five pixels per mm.)

Based on extensive experimentation with ranges up to 40, from arc-shaped band tests symmetric about either  $0^\circ$  or  $45^\circ$ , our main conclusions are two:

- (i) Just above  $\theta = \text{bend}$ , the angle at which an end gets stuck appears to approach  $45^\circ$  as  $\rho$  increases.
- (ii) The viable cones with highest  $\theta$  are symmetric about  $0^\circ$ , with an opening that decreases as  $\rho$  increases.

In this context, it is helpful to speculate about the behavior of semi-infinite band tests under the Euclidean dynamics. Fixing the direction  $\alpha = \pi/2$  for the moment, imagine starting from 1's on

$$E^- = \{(x, y) : x \in (-\infty, 0) \text{ and } 0 < y < 1\},$$

2's on the translate  $E^- - (0, 1)$ , and 0's everywhere else. One expects a critical value  $\text{end}^-(\pi/2) = \text{end}^-(0)$  such that for  $\theta < \text{end}^-(0)$  the maximal  $x$ -coordinate of the excited region tends to  $+\infty$ , whereas for  $\theta > \text{end}^-(0)$  the maximal excited  $x$ -coordinate tends to  $-\infty$ . As a more formal defi-

dition in this context we let  $\text{end}^-(0)$  be the supremum of values of  $\theta$  such that there exists  $(x_n, y_n)$  excited at time  $n$ , with  $x_n \rightarrow \infty$ . We even hazard a guess that at  $\theta = \text{end}^-(0)$  the excited region attains a stable limiting profile as it moves up with asymptotic velocity  $w^-(0)$ . Similarly a cutoff  $\text{end}^+(0)$  and critical velocity  $w^+(0)$  should exist starting from an initial condition semi-infinite in the positive direction. By symmetry of the  $p = \infty$  dynamics, of course, these  $+$  and  $-$  quantities must agree.

For other directions  $\alpha$ , the quantities  $\text{end}^-(\alpha)$  and  $\text{end}^+(\alpha)$  can be defined analogously. By symmetry the two values also agree for  $\alpha = \pi/4$ , and  $\text{end}^+(\alpha) = \text{end}^-(\pi/2 - \alpha)$ , but a little thought leads one to suspect that, typically,

$$\text{end}^-(\alpha) \neq \text{end}^+(\alpha)$$

for  $\alpha \in (0, \pi/4)$ . It is illuminating to rephrase Conjectures 1.6 and 1.7 in terms of  $\text{end}^+$  and  $\text{end}^-$ . The following formulations have the advantage that they should hold for quite general asymmetric sets  $N$ . Since a prebug needs two healthy ends in the same direction, we propose:

**Conjecture 3.1.** *In each direction  $\alpha$ ,*

$$\text{prebug}(\alpha) = \min\{\text{end}^-(\alpha), \text{end}^+(\alpha)\}.$$

For at least one of the two orientations a spiral core spo needs healthy ends in all directions, so we offer:

**Conjecture 3.2.** *For  $\kappa \geq \kappa_0$ ,*

$$\text{spo}_\kappa(p) = \max\{\inf_{\alpha^-} \text{end}^-(\alpha), \inf_{\alpha^+} \text{end}^+(\alpha)\}.$$

Finally, since the trace of a wave fragment can cover a cone between angles  $\alpha^-$  and  $\alpha^+$  as long as ends in those directions are viable and the cone has no problem propagating at locations away from the ends, we believe the following characterization of bug:

**Conjecture 3.3.** *Let*

$$\beta = \min\{\sup_{\alpha^-} \text{end}^-(\alpha^-), \sup_{\alpha^+} \text{end}^+(\alpha^+)\}.$$

*If some closed ring of excitation propagates outward for  $\theta \leq \beta$ , then  $\text{bug}(p) = \beta$ .*

Our experiments with  $p = \infty$ , mentioned above, suggest that  $\text{end}^-$  attains its maximum at  $\alpha = 0$  and its minimum at  $\alpha = \pi/4$ . In light of the symmetries of the square, this scenario makes Conjectures 1.6 and 1.7 consequences of Conjectures 3.1–3.3, the upper bound in (1.3), and our belief that rings propagate for  $\theta \leq \frac{2}{3}$ . See also Remark 4.3.

We conclude this discussion of experimental findings with some speculative curve-fitting. By studying trajectories of band tests such as those shown in Figure 6 for systems with larger ranges, we have extended Table 1 to all  $\rho \leq 40$ . Evaluation of the exact cutoff becomes increasingly delicate as  $\rho$  increases, so there may well be some small errors in our numerical results. But for ballpark estimates we have calculated least-squares fit of estimated data for  $\text{bend}(\rho)$  and  $\text{bug}(\rho)$  over the 36 values  $\rho = 5, \dots, 40$  to curves of the form

$$a + b\rho^{-1} + c\rho^{-2}.$$

Extrapolation to the limit yields the rough guess

$$\text{bend} \approx .653, \quad \text{bug} \approx .657.$$

#### 4. PREBUG UPPER BOUNDS

In this and the next two sections we will deal directly with the Euclidean dynamics obtained by setting  $\theta = \theta_\infty \rho^2$ , scaling space by  $1/\rho$ , and letting  $\rho \rightarrow \infty$ . To formalize the time evolution of the limiting system it is convenient to define a continuum GHM operator  $\mathcal{G}$  that acts on measurable functions  $\varphi : \mathbf{R}^2 \rightarrow \{0, 1, \dots, \kappa - 1\}$ . Denoting by  $|A|$  the area of a set  $A$ , we set

- $\mathcal{G}\varphi(x) = i + 1 \bmod \kappa$  if  $\varphi(x) = i > 0$ ;
- $\mathcal{G}\varphi(x) = 1$  if  $\varphi(x) = 0$  and

$$|\varphi^{-1}(1) \cap (B_p(\rho) + x)| \geq \theta;$$

- $\mathcal{G}\varphi(x) = 0$  otherwise.

In terms of  $\mathcal{G}$ , the time evolution may be succinctly described as  $\xi_{n+1} = \mathcal{G}\xi_n$ . An analogous operator  $\mathcal{C}$  describes the Euclidean CCA.

We feel that Euclidean parallel dynamics constitute a promising new framework for the study of nonlinear spatial systems. If a multistate configuration is represented by a tessellation of space into colored regions with smooth boundaries, the discrete-time dynamics of a transformation such as  $\mathcal{G}$  can be studied in terms of its action on the boundaries. The asymptotic shapes of rings and spirals in excitable cellular automata are studied by this approach in [Gravner and Griffeath 1994]. Our basic task for the remainder of the present paper is the estimation of continuum wave fragments invariant under  $\mathcal{G}$  (or  $\mathcal{C}$ ), an undertaking we refer to informally as bug architecture.

Two simplifying features of the threshold-range scaling limit should be mentioned. First, for  $p = 2$  the action of each update is rotation-invariant. So shapes of continuum rings, spiral wavefronts and symmetric spiral cores are genuinely circular. In particular,  $\text{prebug}(\alpha, 2)$  is independent of  $\alpha$ . Second, since  $B_1(\rho)$  (“diamond”) is a  $45^\circ$  rotation of  $B_\infty(\sqrt{2}\rho/2)$  (“box”), dynamics for the cases  $p = 1$  and  $p = \infty$  are equivalent up to a simple linear transformation. Hence the corresponding cutoffs satisfy

$$\text{spo}(1) = \frac{1}{2} \text{spo}(\infty), \quad \text{bug}(1) = \frac{1}{2} \text{bug}(\infty),$$

and so forth. For this reason we focus only on the case  $p = \infty$  as an extreme instance of anisotropy. We can also take  $\rho = 1$  without loss of generality; we set  $\mathcal{N} = B_p(1)$ .

Given continuous functions  $f < g$  on the interval  $[-l, r]$ , let

$$E = \{(u, v) : u \in [-l, r] \text{ and } f(u) < v < g(u)\}; \tag{4.1}$$

set  $\varphi = 1$  on  $E$ , and  $\varphi = 0$  otherwise.  $E$  is said to define a *prebug of length  $l + r$  and translation  $w$  in direction  $\alpha = 0$*  if  $\mathcal{G}\varphi = 1$  on the translate  $(0, w)$ . To study prebugs in directions  $\alpha \neq 0$ , it is convenient to leave  $f$  and  $g$  alone and rotate the

neighborhood. Let  $\mathcal{N}_\alpha$  be the image of  $\mathcal{N}$  under a counterclockwise rotation through  $\alpha$ , and fix  $w$  so that  $w \geq g(u) - f(u)$  for  $u \in (-l, r)$ . Set

$$h(u, v) = |E \cap ((u, v + w) + \mathcal{N}_\alpha)|. \tag{4.2}$$

Then  $E$  is a *prebug in direction  $\alpha$*  if and only if  $h(u, v) \geq \theta$  for all  $u \in [-l, r]$  and  $f(u) < v < g(u)$ .

Upper bounds on threshold levels that admit prebugs can be obtained by playing off the “top” of a bug against an “end.” Our next three propositions derive the right-hand inequalities of (1.3)–(1.5) by adapting one and the same strategy to the different geometries of box, diamond and circle.

**Proposition 4.1.** *When  $p = \infty$  and  $\alpha = 0$ , prebugs do not exist for  $\theta > \frac{2}{3}$ .*

*Proof.* Let  $E$  be a prebug of translation  $w$  in the direction  $\alpha = 0$ , and let  $\bar{u}$  be a point where  $g$  attains its maximum. There are no points of  $E$  in  $\mathbf{R} \times (g(\bar{u}), \infty)$ , so  $\theta \leq h(\bar{u}, g(\bar{u})) \leq 2(1 - w)$ . Since there are no points of  $E$  in  $(-\infty, -l) \times \mathbf{R}$  and the prebug has translation  $w$ , we must also have  $\theta \leq h(-l, g(-l)) \leq w$ . The two inequalities imply that  $\theta \leq w \leq 1 - \theta/2$ , and hence  $\theta \leq \frac{2}{3}$ .  $\square$

**Proposition 4.2.** *When  $p = \infty$  and  $\alpha = \pi/4$ , prebugs do not exist for  $\theta > \frac{80}{121}$ .*

*Proof.* Let  $E$  be a prebug of translation  $w$  in direction  $\alpha = \pi/4$ , and let  $\bar{u}$  be a point where  $g$  attains its maximum. There are no points of  $E$  in  $\mathbf{R} \times (g(\bar{u}), \infty)$  and the prebug is assumed to have translation  $w$ , so

$$h(\bar{u}, g(\bar{u})) \leq h_1(w), \tag{4.3}$$

where  $h_1(w)$  is the area of the intersection of the strip  $\mathbf{R} \times (-2w, -w)$  with  $\mathcal{N}_{\pi/4}$ . We have  $h_1(w) = (\sqrt{2} - w + \sqrt{2} - \omega)(\omega - w)$ , where  $\omega = \min\{2w, \sqrt{2}\}$ . A simple calculation shows that  $h_1$  is increasing on  $(0, \sqrt{2}/3)$  and decreasing on  $(\sqrt{2}/3, \sqrt{2})$ .

Now consider  $h(-l, g(-l))$ . Any contribution to this area must come from the right half of  $\mathcal{N}_{\pi/4}$ . A glance at Figure 7 shows that

$$h(-l, g(-l)) \leq h_2(w) := \sqrt{2}w - \frac{1}{4}w^2. \tag{4.4}$$

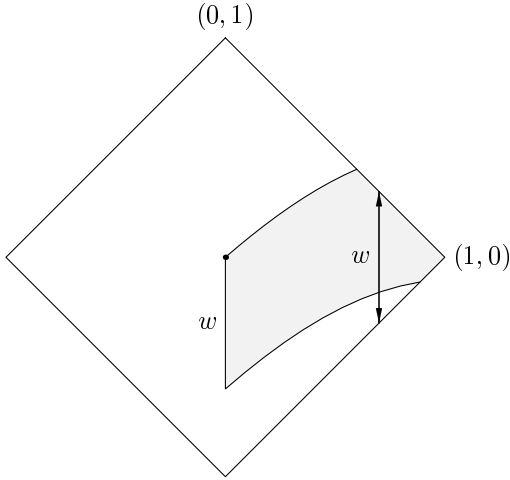


**FIGURE 7.** The diamond's center is  $(-l, g(-l))$ . The area  $h(-l, g(-l))$  of the shaded region is at most  $w(\sqrt{2} - \frac{1}{2}w)$  (bound for the area to the left of the vertical line) plus  $\frac{1}{4}w^2$  (area of the triangle).

The function  $h_2$  is increasing on  $[0, 2\sqrt{2}]$ .

Combining (4.3) and (4.4), we get

$$\theta \leq \max_w \min\{h_1(w), h_2(w)\}.$$

Choose  $w_0 = \frac{4}{11}\sqrt{2}$  so that  $h_1(w_0) = h_2(w_0)$ . Since  $h_1$  is decreasing on  $[w_0, \sqrt{2}]$ , and  $h_2$  is increasing on  $[0, \sqrt{2}]$ , we conclude that  $\theta \leq h_1(w_0) = \frac{80}{121}$  as claimed.  $\square$

**Remark 4.3.** The maximum of  $h_1(w)$  occurs at  $w_1 = \sqrt{2}/3$ , where  $h_1(w_1) = \frac{2}{3}$ . This is the greatest threshold at which an infinite band can reproduce itself in the direction  $\alpha = \pi/4$  under  $p = \infty$  dynamics. In fact, some calculation shows that the most difficult direction for such an infinite band is  $\alpha = \pi/4$ . Imagine starting  $\mathcal{G}$  from a very large ball of 1's on a background of all 0's. The ball should be so big that, as far as  $\mathcal{G}$  is concerned, its boundary is essentially flat in all directions. If  $\theta < \frac{2}{3}$  the ball presumably generates a ring that expands forever with an asymptotic shape. But if  $\theta > \frac{2}{3}$  the resulting ring should break apart in the direction  $\pi/4$  and its images under  $\pi/2$  rotations, and then disintegrate from the ends of its fragments. Thus  $\frac{2}{3}$  is presumably the largest threshold

that can propagate a ring indefinitely for  $p = \infty$ . In the terminology of [FGG], we conjecture that  $\text{ball}(\infty) = \frac{2}{3}$ .

**Proposition 4.4.** When  $p = 2$ , prebugs do not exist for  $\theta > .5335$ .

*Proof.* Once again, let  $E$  be a prebug of translation  $w$  and let  $\bar{u}$  be a point where  $g$  attains its maximum. A reasoning entirely parallel to that of Proposition 4.2, with  $N = N_\alpha$  being the unit disk instead of a diamond, shows that

$$h(\bar{u}, g(\bar{u})) \leq h_1(w) := \int_w^{\min\{2w, 1\}} 2\sqrt{1 - r^2} dr$$

and that

$$h(-l, g(-l)) \leq h_2(w) := tw + 2 \int_t^1 \sqrt{1 - r^2} dr,$$

where  $t = \sqrt{1 - w^2/4}$  is the abscissa of the vertical chord in Figure 8.

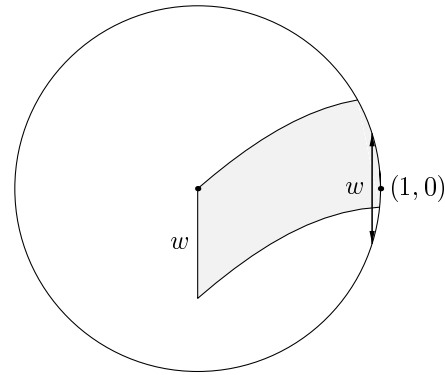


**FIGURE 8.** The area  $h(-l, g(-l))$  of the shaded region is at most  $w\sqrt{1 - w^2/4}$  (bound for the area to the left of the chord) plus the area of the cap delimited by the chord.

Differentiation shows that  $h_1(w)$  is decreasing on  $[\frac{1}{2}, 1]$  and that  $h_2(w)$  is increasing on  $[0, 1]$ . If  $w_0 \approx .547379$  is the solution in  $(\frac{1}{2}, 1)$  of  $h_1(w_0) = h_2(w_0)$ , we conclude as in the proof of Proposition 4.2 that  $\theta \leq h_1(w_0) \approx .5335$ , as claimed.  $\square$

**Remark 4.5.** The maximum of  $h_1(w)$  occurs in  $[0, \frac{1}{2}]$  at the point  $w_1 = 1/\sqrt{5}$ , and a little computation shows that

$$\text{ball}(2) = h_1(w_1) \approx .6435$$

in the terminology of [FGG].

**5. PREBUG AND SPIRAL LOWER BOUNDS for  $p = 2$**

To obtain the lower bound of (1.5) for  $\text{prebug}(\alpha, 2)$ , we will construct a prebug of constant width  $w$  on  $[-(k + 2), (k + 2)]$ , with  $f(x) = g(x) - w$ ,  $g(x) = g(-x)$ , and

$$g(x) = \begin{cases} \sqrt{R^2 - x^2} & \text{if } 0 \leq x \leq k, \\ a - b(x - k) & \text{if } k \leq x \leq k + 2, \end{cases}$$

where  $a = \sqrt{R^2 - k^2}$  and  $b = k/\sqrt{R^2 - k^2}$ , so that  $g$  has a continuous derivative. The general approach we take is the following: first pick  $b$  and  $w$  to take care of the end of the prebug, then choose  $R$  large enough to take care of the middle, and finally define  $k$  and  $a$  to solve the above equations.

Let  $r = l = k + 2$ ; define  $E$  (4.1) by

$$E = \{(u, v) : u \in [-l, l] \text{ and } g(u) - w < v < g(u)\},$$

and define

$$h(x, v) = |E \cap ((x, g(x) + v) + \mathcal{N})|.$$

(this differs from (4.2) in that the second argument indicates vertical displacement from the top of the bug, rather than absolute position). For  $E$  to be a prebug we need  $h(x, v) \geq \theta$  for  $x \in [0, l]$  and  $v \in [0, w]$ . The next three lemmas show that, for large  $R$ , it suffices to check this inequality at the three points  $(l, 0)$ ,  $(l, w)$  and  $(0, w)$ . Let  $\sigma(v, c)$  be the area of the portion of  $\mathcal{N}$  between the lines  $y = -cx - v$  and  $y = -cx - v - w$  (Figure 9).

**Lemma 5.1.** *If  $R$  is sufficiently large, to conclude that  $E$  is a prebug it suffices to check that*

- (i)  $h(l, v) \geq \theta$  for  $v \in [0, w]$ , and
- (ii)  $\sigma(v, c) > \theta$  for all  $v \in [0, w]$  and  $c \in [0, b]$ .

*Proof.* For  $u \in [l - 1, l]$  we have  $h(u, v) \geq h(l, v)$ , because, over this range of values of  $u$ , sliding the

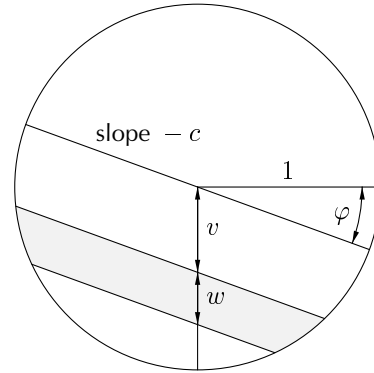


**FIGURE 9.** The shaded area is  $\sigma(v, c)$ . We have  $\sigma(v, c) \geq \sigma(w, 0)$  for  $v \in [0, w]$  and  $c \in [0, b]$  (see the proof of Lemma 5.3).

disk  $(u, g(u) + v) + \mathcal{N}$  to the left along lines of constant  $v$  can only increase the intersection with  $E$ . Thus (i) implies  $h(u, v) \geq \theta$  for  $u \in [l - 1, l]$ .

To study the range  $u \in [0, l - 1]$ , suppose (ii) holds. Since  $\sigma$  is continuous, there is an  $\varepsilon > 0$  such that  $\sigma(v, c) \geq \theta + \varepsilon$  for  $v \in [0, w]$  and  $c \in [0, b]$ . For  $R$  large enough we can approximate  $E$  locally by a straight band of slope  $g'(u)$ , and write

$$h(u, v) \geq \sigma(v, -g'(u)) - \varepsilon \geq \theta$$

for all  $u \in [0, l - 1]$  and  $v \in [0, w]$ . □

**Lemma 5.2.** *Property (i) of Lemma 5.1 holds provided that  $h(l, 0) \geq \theta$  and  $h(l, w) \geq \theta$ .*

*Proof.* Let  $i(v) = |\{x \leq 0 : (x, -v - bx) \in \mathcal{N}\}|$ , where  $|\cdot|$  represents length in  $\mathbf{R}^1$ . It is easy to see that

$$\frac{\partial}{\partial v} h(l, v) = -i(v) + i(v + w).$$

Now  $i(b) = 1$ , and  $i(v)$  is increasing on  $[-1, b]$  and decreasing on  $[b, 1]$ , so if we let  $v_0$  be the point in  $[-1, b]$  where  $i(v_0) = i(v_0 + w)$ , then  $h(l, v)$  is increasing on  $[-1, v_0]$  and decreasing on  $[v_0, 1]$ . Thus the minimum of  $h(l, v)$  over  $[0, w]$  must be attained at an endpoint. □

**Lemma 5.3.** *Property (ii) of Lemma 5.1 holds provided that  $\sigma(w, 0) > \theta$ .*

*Proof.* If  $\varphi = \arctan c$  is the angle that the line  $-v - cx$  makes with the  $x$ -axis, then

$$\sigma(v, c) = \int_{v \cos \varphi}^{\min\{(v+w) \cos \varphi, 1\}} 2\sqrt{1-r^2} dr$$

(see Figure 9). From this it is clear that increasing  $v$  decreases the integral. Setting  $v = w$  and  $z = w \cos \varphi$ , the right side becomes

$$\int_z^{\min\{2z, 1\}} 2\sqrt{1-r^2} dr,$$

which is increasing as a function of  $z$  on  $[0, 1/\sqrt{5}]$  and decreasing on  $[1/\sqrt{5}, 1]$  (compare Remark 4.5). Changing variables, we conclude that the minimum of  $\sigma(w, c)$  for  $c \in [0, b]$  occurs at an endpoint. The proof of Lemma 5.1 shows that

$$\sigma(w, b) = h(l - 1, w) > \theta,$$

so we only need to worry about  $\sigma(w, 0)$ . □

**Proposition 5.4.** *When  $p = 2$ , there are prebugs (of constant width) for  $\theta < .5199$ .*

*Proof.* Let  $\varphi = \arctan b$ . By Lemmas 5.1–5.3, in order to manufacture the desired prebug it suffices to pick  $w$  and  $\varphi$  so that  $\sigma(w, 0)$ ,  $h(l, 0)$ , and  $h(l, w)$  are all at least .5199. From the proof of Lemma 5.3 we have

$$\sigma(w, 0) = \int_w^{\min\{2w, 1\}} 2\sqrt{1-r^2} dr.$$

Consulting Figure 10 we see that

$$h(l, 0) = \int_0^{w \cos \varphi} \sqrt{1-r^2} dr + \frac{1}{2} w^2 \sin \varphi \cos \varphi,$$

$$h(l, w) = \int_{w \cos \varphi}^{2w \cos \varphi} \sqrt{1-r^2} dr + \frac{3}{2} w^2 \sin \varphi \cos \varphi - A,$$

where  $A$  is the area of the black region in Figure 10. To compute  $A$ , we observe that if  $-x_0$  is the abscissa of the leftmost point  $P$  of the black region, then

$$A = \frac{x_0}{2} \left( 2w + \sqrt{1-x_0^2} \right) - \int_0^{x_0} \sqrt{1-r^2} dr.$$

The last four expressions are tedious to deal with by hand but can be easily evaluated by computer.

Taking  $w = .555515$  and  $\varphi = .57115$  gives the desired bound. □

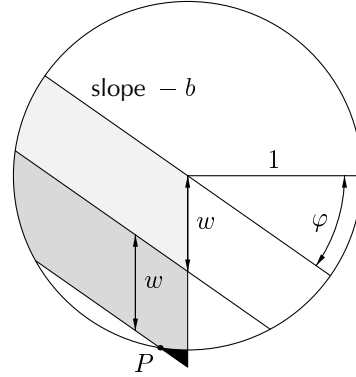


**FIGURE 10.** The lightly and darkly shaded regions have area  $h(l, 0)$  and  $h(l, w)$ , respectively. The black region sticking out of the circle has area  $A$ .

As advertised in the introduction, we now construct an spo by shaving a little off our isotropic prebug and arranging its rotations in a circle.

*Proof of Theorem 1.5 for  $p = 2$ .* Let  $\mathcal{R}_\alpha$  denote rotation through an angle  $\alpha$ . Let  $E$  be a bug of width  $w$  defined on  $[-l, l]$ , and let  $M$  be a large number chosen so that  $\alpha = \arcsin(w/(M + l)) = 2\pi/\kappa$  for some integer  $\kappa$ . Set

$$B = E + (M, 0),$$

$$B' = (B + (0, w)) \cap \mathcal{R}_\alpha B,$$

$$B'' = \mathcal{R}_{-\alpha} B' \subset B.$$

Finally, write  $\varepsilon(M) = |B| - |B''|$ . When  $M$  is large, rotation by  $\alpha$  and translation by  $(0, w)$  almost coincide, so  $\varepsilon(M) \rightarrow 0$  as  $M \rightarrow \infty$ . Since  $E$  is a prebug for threshold  $\theta$ , if we decrease the threshold to  $\theta - \varepsilon(M)$  and start with 1's on  $B''$  and 0's on  $B'$ , then at time 1 we will have 1's on  $B'$ . For  $0 \leq j \leq \kappa$ , set  $R_j = \mathcal{R}_{-j\alpha} B''$  and let  $\xi(x) = j$  on  $R_j$ . From the last observation and the rotation invariance of the limiting dynamics in the case  $p = 2$ , it follows that  $\xi$  defines a  $\kappa$ -color spo for threshold  $\theta - \varepsilon(M)$ . As noted in the introduction, by choosing  $\kappa$  to be a multiple of  $\kappa_0$  we can also construct a  $\kappa_0$ -color spo for any  $\kappa_0 \geq 3$ . □

**6. PREBUG AND SPIRAL LOWER BOUNDS for  $p = \infty$**

The strategy for  $p = \infty$  parallels that for  $p = 2$  except that now, in order to make an spo, we need to construct different prebugs for different directions  $\alpha$ . As in Section 4, we will leave the prebug alone and rotate the neighborhood. Let  $\mathcal{N}_\alpha$  be the set that results when the  $p = \infty$  box  $\mathcal{N}$  is rotated counterclockwise through  $\alpha$ , and suppose without loss of generality that  $0 \leq \alpha \leq \pi/4$ . To obtain a lower bound for the existence of prebugs, we will design prebugs of constant width  $w$  on  $[-(j + 4), (k + 4)]$  with

$$g(x) = \begin{cases} a_0 - b_0(x + j) & \text{if } -j - 4 \leq x \leq -j, \\ \sqrt{R^2 - x^2} & \text{if } -j \leq x \leq k, \\ a_1 - b_1(x - k) & \text{if } k \leq x \leq k + 4, \end{cases}$$

where  $a_0 = \sqrt{R^2 - j^2}$ ,  $b_0 = j/\sqrt{R^2 - j^2}$ ,  $a_1 = \sqrt{R^2 - k^2}$  and  $b_1 = k/\sqrt{R^2 - k^2}$  are chosen so that  $g$  has a continuous derivative. Our general strategy is as follows: first pick  $b_0$  and  $w$  to take care of the left end of the prebug, then pick  $b_1$  to take care of the right end, then choose  $R$  large enough to handle the middle, and finally determine  $j$ ,  $k$ ,  $a_0$  and  $a_1$  by solving the above equations.

Write  $l = j + 4$ ,  $r = k + 4$ ,

$$E = \{(u, v) : u \in [-l, r] \text{ and } g(u) - w < v < g(u)\},$$

and  $h(x, v) = |E \cap ((x, g(x) + v) + \mathcal{N}_\alpha)|$ . To check that  $E$  defines a prebug in direction  $\alpha$ , we have to verify that  $h(x, v) \geq \theta$  for  $x \in [-l, r]$  and  $v \in [0, w]$ . The next three lemmas serve to reduce the number of points  $(x, v)$  that we need to check. Once more, let  $\sigma(v, c)$  be the area of the portion of  $\mathcal{N}$  between the lines  $y = -cx - v$  and  $y = -cx - v - w$  (Figure 11). The first two lemmas are almost the same as their counterparts in Section 5.

**Lemma 6.1.** *If  $R$  is sufficiently large, to conclude that  $E$  is a prebug it suffices to check that*

- (i)  $h(r, v) \geq \theta$  and  $h(-l, v) \geq \theta$  for all  $v \in [0, w]$ , and
- (ii)  $\sigma(v, c) > \theta$  for all  $v \in [0, w]$  and  $c \in [-b_0, b_1]$ .

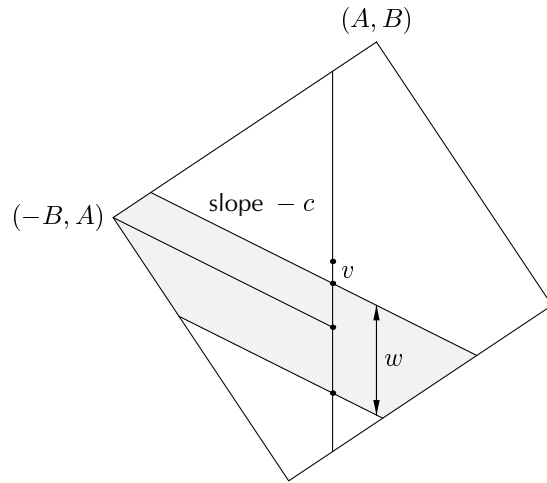


**FIGURE 11.** The shaded area is  $\sigma(v, c)$ . The points marked on the vertical line have ordinate  $0, -v, -v_0$  and  $-v - w$  (from the top down).

*Proof.* Using the same reasoning as in the proof of Lemma 5.1 (and its mirror image), we see that  $h(u, v) \geq h(r, v)$  for  $u \in [r - 2, r]$  and  $h(u, v) \geq h(-l, v)$  for  $u \in [-l, -l + 2]$ . Thus (i) implies  $h(u, v) \geq \theta$  for  $u \in [r - 2, r] \cup u \in [-l, -l + 2]$ . Similarly, (ii) implies that  $h(u, v) \geq \theta$  for all  $u \in [-l + 2, r - 2]$  and  $v \in [0, w]$ , by the reasoning in the proof of Lemma 5.1.  $\square$

**Lemma 6.2.** *Property (i) of Lemma 6.1 holds provided that  $h(r, 0) \geq \theta$ ,  $h(r, w) \geq \theta$ ,  $h(-l, 0) \geq \theta$  and  $h(-l, w) \geq \theta$ .*

*Proof.* We first show that  $h(r, 0) \geq \theta$  and  $h(r, w) \geq \theta$  imply  $h(r, v) \geq \theta$  for  $v \in [0, w]$ . Let  $i(v) = |\{x \leq 0 : (x, -v - b_1x) \in \mathcal{N}_\alpha\}|$ . Then

$$\frac{\partial}{\partial v} h(r, v) = -i(v) + i(v + w).$$

Let  $(A, B)$  be the corner of  $\mathcal{N}_\alpha$  in the first quadrant (Figure 11). Pick  $v_0$  so that  $-v_0 - b_1(-B) = A$ . Now  $i(v_0) = B$ , and  $i(v)$  is increasing on  $[-\infty, v_0]$  and decreasing on  $[v_0, \infty]$ , so if we let  $v_1$  be the point in  $[-\infty, v_0]$  where  $i(v_1) = i(v_1 + w)$ , then  $h(l, v)$  is increasing on  $[-\infty, v_1]$  and decreasing on  $[v_1, \infty]$ . Thus the minimum of  $h(l, v)$  over  $[0, w]$  must be attained at an endpoint. An analogous argument proves that  $h(-l, 0) \geq \theta$  and  $h(-l, w) \geq \theta$  imply  $h(-l, v) \geq \theta$  for  $v \in [0, w]$ .  $\square$

The next result is weaker than the corresponding Lemma 5.3 for a simple reason: when  $0 < \alpha < \pi/4$ , the minimum of  $\sigma(c, w)$  does not occur at  $c = 0$ .

**Lemma 6.3.** *Property (ii) of Lemma 5.1 holds provided that  $\sigma(w, c) > \theta$  for  $c \in [-b_0, b_1]$ .*

*Proof.* Let  $j(v) = |\{x : (x, -v - cx) \in \mathcal{N}_\alpha\}|$ . It is easy to see that

$$\frac{\partial}{\partial v} \sigma(v, c) = -j(v) + j(v + w).$$

Define  $v_2$  by requiring that the line  $y = -v - cx$  intersect two opposite sides of the rotated square if and only if  $v \in [-v_2, v_2]$ . It is easy to see that  $j(v)$  is constant on  $[0, v_2]$  and decreasing on  $[v_2, \infty]$  so  $\partial\sigma/\partial v \leq 0$ . (See Figure 11. For the slope pictured there,  $v_2 = v_0$ . However, if  $c = 0$ , then  $v_2 = -v_0$ .)  $\square$

We are now ready to prove the lower bounds of (1.3) and (1.4).

**Proposition 6.4.** *When  $p = \infty$  and  $\alpha = 0$ , prebugs of constant width exist for  $\theta \leq .6339$ .*

*Proof.* We take  $a_0 = a_1, b_0 = b_1 = b$ , and  $j = k$ . For  $w > \frac{1}{2}$  and  $b > 1$ , we have

$$h(-l, 0) = w - \frac{(b - 1)^2}{2b}$$

and

$$h(-l, w) = w - \frac{(2w - 1)^2}{2b},$$

as can be seen from Figure 12. Choosing  $b = 2w$  we get  $h(-l, 0) = h(-l, w) = (4w - 1)/4w$ . Now  $\sigma(w, 0) = 2(1 - w)$ , so to make all three areas equal, set  $(4w - 1)/4w = 2(1 - w)$ . Solving for  $w$  gives  $w = (1 + \sqrt{3})/4 \approx .68301$ , in which case all three areas are

$$2(1 - w) = (3 - \sqrt{3})/2 \approx .63397.$$

This candidate for a prebug has  $b = 2w = \frac{1}{2}(1 + \sqrt{3})$ . By Lemmas 6.2 and 6.3, in order to complete the proof we must show that for the chosen  $w$  the minimum of  $\sigma(w, c)$  over  $0 \leq c \leq b$  occurs at  $c = 0$ . A routine analysis of the three possible intersection

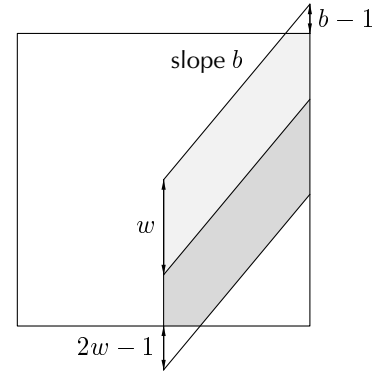


**FIGURE 12.** The lightly and darkly shaded regions have area  $h(-l, 0)$  and  $h(-l, w)$ , respectively.

configurations confirms this (when both edges of the strip intersect the square one must use the fact that  $w > \frac{2}{3}$ ).  $\square$

**Proposition 6.5.** *When  $p = \infty$  and  $\alpha = \pi/4$ , prebugs of constant width exist for  $\theta \leq .6355$ .*

*Proof.* Again take  $a_0 = a_1, b_0 = b_1$ , and  $j = k$ . To prepare for the cases  $0 < \alpha < \pi/4$ , which will be analyzed later in this section, we now develop general formulas for the areas of certain strips. Let  $(A, B)$  be the corner of  $\mathcal{N}_\alpha$  that is in the first quadrant. The sides of our rotated rectangle have defining equations  $s_j x + t_j$ , for  $j = 0, 1, 2, 3$ , where

$$\begin{aligned} s_0 &= s_3 = \frac{B - A}{A + B}, \\ s_1 &= s_2 = \frac{A + B}{A - B}, \\ t_0 &= \frac{2}{A + B}, \quad t_3 = -t_0, \\ t_1 &= \frac{2}{A - B}, \quad t_2 = -t_1 \end{aligned}$$

(see Figure 13). For  $i = 0, 1, 2$  we refer to  $-i w - cx$  as *line i*, and denote by

$$x_{ij} = \frac{-t_j - iw}{s_j + c} \tag{6.1}$$

the coordinate of the intersection of line  $i$  with side  $j$ . To compute  $\sigma(w, c)$  we consider two cases, as shown in Figure 14.

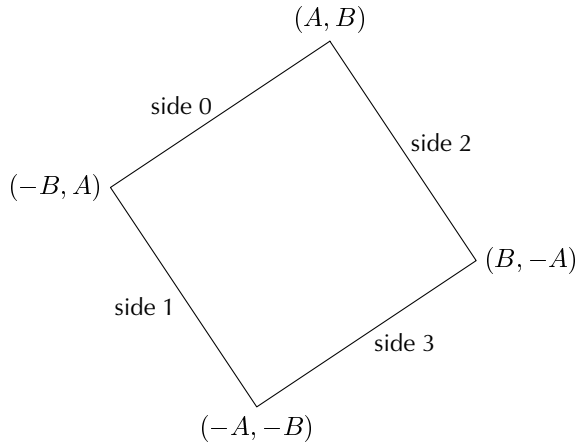


FIGURE 13. Numbering of the sides of  $N_\alpha$ .

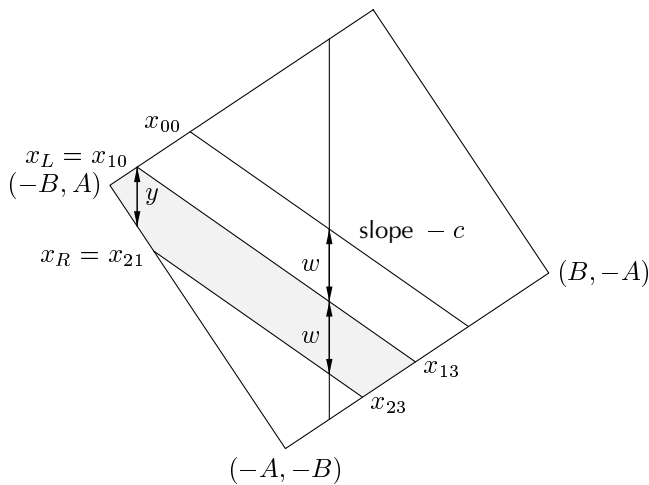
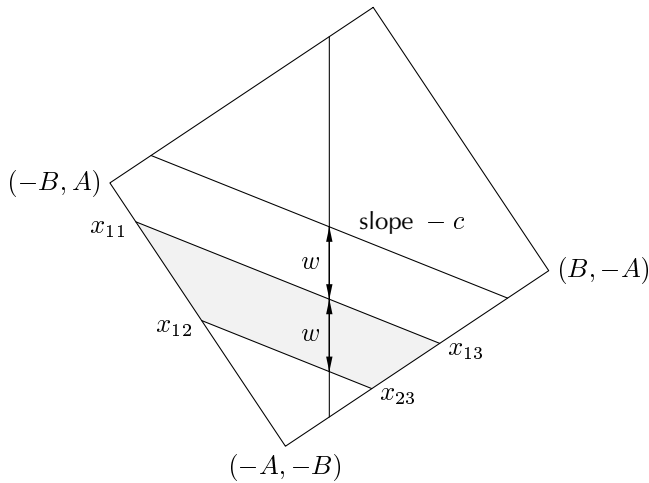


FIGURE 14. Computation of the shaded area  $\sigma(w, c)$ .

In Case 1 we have  $-w + cB < -A$ ,  $-2w + cA > -B$ ,  $-w + cB < -A$ . Then

$$\sigma(w, c) = \frac{1}{2}(x_{21} - x_{11})w + (x_{23} - x_{21})w + \frac{1}{2}(x_{13} - x_{23})w.$$

In Case 2 we have  $-w + cB > A > -2w + cB$ ,  $-2w + cA > -B$ ,  $-w - cB < -A$ . Then

$$\sigma(w, c) = \frac{1}{2}(x_{13} - x_{23}) + (x_{23} - x_R)w + \frac{1}{2}(x_R - x_L)(y + w) + \frac{1}{2}(x_L + B)y,$$

where  $x_R = \max\{x_{10}, x_{21}\}$ ,  $x_L = \min\{x_{10}, x_{21}\}$ , and  $y = (s_0x_L + t_0) - (s_1x_L + t_1)$ .

For  $\alpha = \pi/4$  (that is,  $A = 0$ ) the slope  $b$  we choose for the end of our prebug will place us in Case 2, so that, consulting Figure 14, we obtain

$$\begin{aligned} h(-l, 0) &= h(r, 0) = -x_{00}w + \frac{1}{2}(x_{00} - x_{01})w, \\ h(-l, w) &= h(r, w) = -x_Rw + \frac{1}{2}(x_R - x_L)(y + w) \\ &\quad + \frac{1}{2}(x_L + B)y. \end{aligned}$$

These last formulas are not pleasant to manipulate by hand, but with the computer one finds that for  $w = .573211$  and  $b = .533933$  the values of  $h(-l, 0)$ ,  $h(-l, w)$  and  $\sigma(w, 0)$  are all at least  $.63557$ . In view of Lemmas 6.1–6.3, the proof will be complete once we check that the minimum of  $\sigma(w, c)$  over  $[0, b]$  occurs at an endpoint. (Recall that  $\sigma(w, b) \geq h(r - 2, w) = h(-l + 2, w) > \theta$ , using Lemma 6.1.)

To evaluate  $\partial\sigma/\partial c$  we will not attack the formulas directly, but instead observe that by changing from  $c$  to  $c + \Delta$  we gain and lose two triangles, so in Case 1, ignoring terms of order  $\Delta^2$ ,

$$\frac{\partial\sigma}{\partial c} = \frac{(x_{11}^2 - x_{21}^2 + x_{23}^2 - x_{13}^2)}{2}.$$

Now when  $A = 0$  and  $B = \sqrt{2}$ , we have  $s_0 = s_3 = 1$ ,  $s_1 = s_2 = -1$ ,  $t_0 = t_2 = \sqrt{2}$ ,  $t_1 = t_3 = -\sqrt{2}$ , so

$$\begin{aligned} x_{11} &= \frac{\sqrt{2} - w}{-1 + c}, & x_{13} &= \frac{\sqrt{2} - w}{1 + c}, \\ x_{21} &= \frac{\sqrt{2} - 2w}{-1 + c}, & x_{23} &= \frac{\sqrt{2} - 2w}{1 + c}, \end{aligned}$$

and

$$\frac{\partial \sigma}{\partial c} = \frac{1}{2}((\sqrt{2}-w)^2 - (\sqrt{2}-2w)^2) \left( \frac{1}{(1-c)^2} - \frac{1}{(1+c)^2} \right),$$

which is positive. In Case 2,

$$\frac{\partial \sigma}{\partial c} = \frac{x_{10}^2 - x_{21}^2 + x_{23}^2 - x_{13}^2}{2}$$

and  $x_{10} = (-\sqrt{2} - w)/(1 + c)$ , so

$$\frac{\partial \sigma}{\partial c} = \frac{\mu}{(1+c)^2} - \frac{\nu}{(1-c)^2},$$

where  $\mu = \frac{1}{2}((\sqrt{2}+w)^2 - (\sqrt{2}-w)^2 + (\sqrt{2}-2w)^2) = 1 + 2w^2$ , and  $\nu = \frac{1}{2}(\sqrt{2} - 2w)^2$ . The right side is positive when  $(1 - c)/(1 + c) > \sqrt{\nu/\mu}$  and negative when  $(1 - c)/(1 + c) < \sqrt{\nu/\mu}$ , so  $\sigma(w, c)$  increases and then decreases in  $[0, b]$ . Hence the minimum is attained at an end point, which finishes the proof.  $\square$

We now turn to lower bounds for  $0 < \alpha < \pi/4$ . Our first goal is to show that to verify the hypothesis of Lemma 6.3, it suffices to check the value of  $\sigma(w, c)$  at one point. As in the proofs of Propositions 6.4 and 6.5, it is useful to know a little about the prebugs in question in order to reduce the number of cases we have to consider, so we will describe them now. For historical reasons we will let  $\beta = \pi/4 - \alpha$  and  $\gamma = 1 - 4\alpha/\pi \in [0, 1]$ . Table 2 lists the choices of  $w$ ,  $b_0$ , and  $b_1$  for our prebugs (which suffices to describe them modulo the choice of a sufficiently large  $R$ ) for 30 values of  $\gamma$ . We extend these choices to all  $\gamma \in [0, 1]$  by declaring that they are piecewise linear and continuous. The column of the table that gives the associated thresholds  $\theta$  should explain why we use a finer grid near  $\gamma = .84$ . *For the rest of the paper, our case analysis refers to the prebugs of Table 2.*

**Lemma 6.6.** *Let  $w(\alpha)$ ,  $b_0(\alpha)$ , and  $b_1(\alpha)$ , for  $\alpha \in (0, \pi/4)$ , be defined by Table 2 and linear interpolation. For each  $\alpha : 0 < \alpha < \pi/4$  there is a constant  $c_\alpha$  such that  $\sigma(w, c)$  is increasing and then decreasing on  $[-b_0(\alpha), c_\alpha]$  and on  $[c_\alpha, b_1(\alpha)]$ . Hence to*

*verify the hypothesis of Lemma 6.3 it suffices to check that  $\sigma(w(\alpha), c_\alpha) > \theta$ .*

*Proof.* To evaluate  $\sigma(w, c)$  for  $c \geq 0$  there are five cases to consider, as indicated by Figure 15. We begin by evaluating the derivative of  $\sigma$  in each of the five cases.

In Case 1 we have

$$\frac{\partial \sigma}{\partial c} = \frac{x_{11}^2 - x_{12}^2}{2}.$$

Recalling (6.1) and the choices  $s_2 = s_1$ ,  $t_2 = -t_1 > 0$ , we see that the right side equals

$$\frac{(t_1 + w)^2}{(s_1 + c)^2} - \frac{(t_2 + w)^2}{(s_1 + c)^2} < 0.$$

In Case 2a,

$$\frac{\partial \sigma}{\partial c} = \frac{x_{11}^2 - x_{13}^2}{2},$$

with  $x_{11}^2$  increasing and  $x_{13}^2$  decreasing, so in this case  $\sigma$  is decreasing and then increasing. (In the last statement, and similar claims below, we allow the possibility that one of the cases is empty, i.e., that  $\sigma$  is monotone over the interval.)

In Case 2b,

$$\frac{\partial \sigma}{\partial c} = \frac{x_{11}^2 - x_{21}^2 - x_{12}^2 + x_{23}^2}{2}.$$

Note that in deriving this formula there are two alternatives to consider ( $x_{23} \leq 0$ ,  $x_{23} > 0$ ), but the formula is the same for either. Similar remarks apply to Cases 3 and 4. Plugging in (6.1), and using the fact that  $s_2 = s_1$ , the right side becomes

$$\frac{(t_1 + w)^2}{(s_1 + c)^2} - \frac{(t_1 + 2w)^2}{(s_1 + c)^2} - \frac{(t_2 + w)^2}{(s_1 + c)^2} + \frac{(t_3 + 2w)^2}{(s_3 + c)^2}.$$

To check this and the two similar formulas below, note that the coefficients of  $w$  alternate  $(1, 2, 1, 2)$  and that the subscripts of  $t$  and  $s$  agree with the second subscript of  $x$ . Rearranging, we see that the area is decreasing when

$$\frac{(s_1 + c)^2}{(s_3 + c)^2} < \frac{(t_1 + 2w)^2 + (t_2 + w)^2 - (t_1 + w)^2}{(t_3 + 2w)^2}.$$

$\gamma$	$A$	$B$	$w$	$b_0$	$b_1$	$\theta$	$\sigma(w_\alpha, c_\alpha)$	$g(-l, 0)$	$g(-l, w)$	$g(r, 0)$	$g(r, w)$
0.00	0.000	1.414	0.57321	0.53393	0.53393	0.63557					
0.05	0.056	1.413	0.57530	0.51478	0.55985	0.63448	0.63448	0.63449	0.63449	0.63934	0.63934
0.10	0.111	1.410	0.57805	0.49824	0.58750	0.63335	0.63335	0.63336	0.63335	0.64322	0.64323
0.15	0.166	1.404	0.58150	0.48481	0.61688	0.63215	0.63215	0.63215	0.63215	0.64726	0.64726
0.20	0.221	1.397	0.58574	0.47533	0.64807	0.63080	0.63081	0.63080	0.63080	0.65150	0.65151
0.25	0.276	1.387	0.59098	0.47171	0.68126	0.62915	0.62915	0.62915	0.62915	0.65612	0.65612
0.30	0.330	1.375	0.59752	0.47700	0.71693	0.62693	0.62693	0.62693	0.62693	0.66126	0.66127
0.35	0.384	1.361	0.60402	0.48395	0.75458	0.62504	0.62504	0.62505	0.62504	0.66538	0.66538
0.40	0.437	1.345	0.61024	0.49110	0.79406	0.62369	0.62369	0.62369	0.62370	0.66822	0.66822
0.45	0.489	1.327	0.61623	0.49864	0.83542	0.62290	0.62290	0.62290	0.62290	0.66986	0.66986
0.50	0.541	1.307	0.62200	0.50675	0.87838	0.62267	0.62268	0.62267	0.62267	0.67033	0.67033
0.55	0.592	1.284	0.62757	0.51563	0.92236	0.62304	0.62305	0.62304	0.62305	0.66971	0.66970
0.60	0.642	1.260	0.63373	0.53475	0.96831	0.62329	0.62330	0.62329	0.62329	0.66860	0.66860
0.65	0.691	1.234	0.64069	0.57703	1.01657	0.62230	0.62308	0.62230	0.62230	0.66718	0.66718
0.70	0.739	1.206	0.64944	0.65833	1.06854	0.62046	0.62082	0.62046	0.62045	0.66611	0.66610
0.75	0.786	1.176	0.65833	0.78677	1.12223	0.61715	0.61715	0.61767	0.61715	0.66425	0.66425
0.80	0.831	1.144	0.66578	0.88897	1.17521	0.61351	0.61351	0.62165	0.61351	0.66068	0.66068
0.81	0.840	1.138	0.66713	0.91107	1.18572	0.61307	0.61307	0.62278	0.61305	0.65979	0.65979
0.82	0.849	1.131	0.66846	0.93217	1.19624	0.61271	0.61271	0.62418	0.61271	0.65887	0.65887
0.83	0.858	1.124	0.66974	0.95617	1.20670	0.61249	0.61249	0.62554	0.61248	0.65789	0.65789
0.84	0.867	1.117	0.67098	0.98217	1.21713	0.61239	0.61239	0.62696	0.61238	0.65686	0.65686
0.85	0.876	1.111	0.67218	1.01027	1.22751	0.61242	0.61242	0.62846	0.61242	0.65579	0.65579
0.86	0.884	1.104	0.67332	1.04187	1.23781	0.61262	0.61262	0.62997	0.61260	0.65466	0.65466
0.87	0.893	1.097	0.67441	1.07597	1.24802	0.61296	0.61296	0.63161	0.61295	0.65348	0.65348
0.88	0.901	1.090	0.67543	1.11617	1.25812	0.61349	0.61349	0.63320	0.61348	0.65225	0.65224
0.89	0.910	1.083	0.67639	1.14727	1.26811	0.61420	0.61420	0.63558	0.61419	0.65095	0.65096
0.90	0.918	1.075	0.67726	1.19837	1.27791	0.61513	0.61513	0.63704	0.61513	0.64960	0.64960
0.95	0.960	1.038	0.68024	1.38867	1.32369	0.62346	0.62346	0.62362	0.62346	0.64188	0.64188
1.00	1.000	1.000	0.68301	1.36602	1.36602	0.63397					

**TABLE 2.** The columns headed  $A$ ,  $B$ ,  $w$ ,  $b_0$ ,  $b_1$  and  $\theta$  prescribe the design specifications for the family of prebug candidates used in the proof of Theorem 1.5. The remaining columns list the five “vital statistics” that, according to Lemmas 6.1–6.6, ensure that these candidates are all legitimate prebugs for  $\theta = .6123$ . See also the section on software availability at the end of this paper.

Since  $(s_1 + c)^2 / (s_3 + c)^2$  is decreasing on  $(-s_3, -s_1)$ , it follows that within Case 2b the area  $\sigma$  increases and then decreases.

In Case 3 we have

$$\frac{\partial \sigma}{\partial c} = \frac{x_{11}^2 - x_{21}^2 - x_{13}^2 + x_{23}^2}{2}.$$

Substituting (6.1), the right side becomes

$$\frac{(t_1 + w)^2}{(s_1 + c)^2} - \frac{(t_1 + 2w)^2}{(s_1 + c)^2} - \frac{(t_3 + w)^2}{(s_3 + c)^2} + \frac{(t_3 + 2w)^2}{(s_3 + c)^2}.$$

The intercept  $t_1$  is less than 0 and within Case 3 we must have  $2w < -t_1$ , which implies that  $t_1 + w < t_1 + 2w < 0$ . Rearranging, we see that the area is decreasing when

$$\frac{(s_3 + c)^2}{(s_1 + c)^2} < \frac{(t_3 + w)^2 - (t_3 + 2w)^2}{(t_1 + w)^2 - (t_1 + 2w)^2}.$$

Now  $(s_3 + c)^2 / (s_1 + c)^2$  is increasing on the interval  $(-s_3, -s_1)$ , so  $\sigma$  is decreasing and then increasing in Case 3.

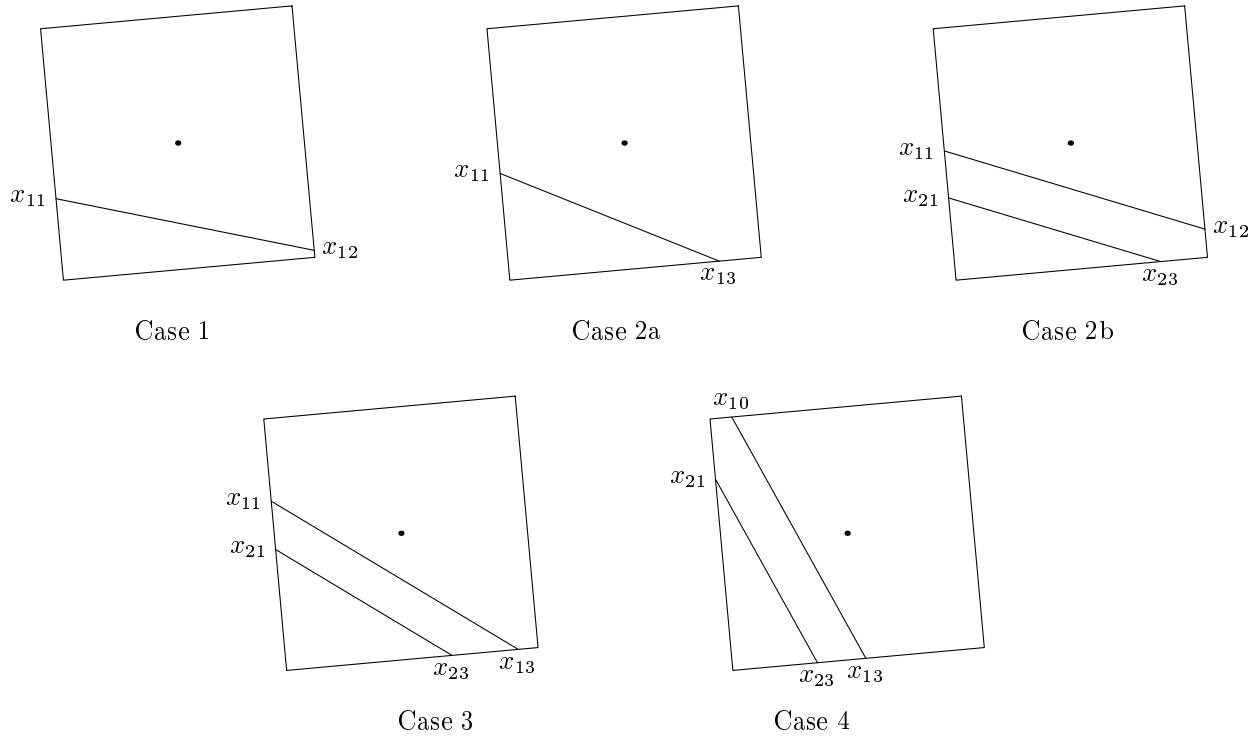


FIGURE 15. Intersection configurations for the proof of Lemma 6.6.

Finally, in Case 4 we have

$$\frac{\partial \sigma}{\partial c} = \frac{x_{10}^2 - x_{21}^2 - x_{13}^2 + x_{23}^2}{2}.$$

By (6.1), and since  $s_0 = s_3$ , the right side equals

$$\frac{(t_0 + w)^2}{(s_3 + c)^2} - \frac{(t_1 + 2w)^2}{(s_1 + c)^2} - \frac{(t_3 + w)^2}{(s_3 + c)^2} + \frac{(t_3 + 2w)^2}{(s_3 + c)^2}.$$

Rearranging, we see that the area is decreasing when

$$\frac{(s_3 + c)^2}{(s_1 + c)^2} > \frac{(t_0 + w)^2 + (t_3 + 2w)^2 - (t_3 + w)^2}{(t_1 + 2w)^2}.$$

Since  $(s_3 + c)^2/(s_1 + c)^2$  is increasing, within Case 4 the area  $\sigma$  increases and then decreases.

We can now identify the  $c_\alpha$  in the statement of the lemma. For  $A$  close to 0,  $w > A$  and  $2w < B$ , so we start with Case 3 when  $c = 0$ . In that case  $\sigma$  is d-i (decreasing then increasing) in Case 3 and i-d in Case 4; taking  $c_\alpha$  to be the minimum in Case 3, the desired conclusion holds on  $[0, b_1]$ .

When  $A$  is close to 1,  $w < A$  and  $2w > B$ , so we start in Case 1 (when  $c = 0$ ) where  $\sigma$  is decreasing. Case 1 can lead to either Case 2a or 2b. If 2a comes first, two sequences can occur:

Case 1	Case 2a	Case 3	Case 4
d	d-i	i	i-d
d	d	d-i	i-d

The derivative of  $\sigma$  is continuous so the signs must match at the transitions between cases. If Case 2b comes first, then the second row is the only possibility since  $\sigma$  is i-d in Case 2b. For either of the situations depicted, taking  $c_\alpha$  to be the first minimum (which may occur in Case 2a or Case 3), the desired conclusion holds on  $[0, b_1]$ .

The final possibility one needs to consider, which occurs for  $A$  near .645, is that  $\sigma$  starts in Case 2a or 2b. But this situation can be analyzed by simply deleting the first column above.

The details are similar but simpler when  $c < 0$ . There are two more cases to consider: lines 1 and 2

intersect side 2, and line 2 intersects side 1 or side 3. As in the five cases considered above, there is at most one critical point within any case, so it is only a question of checking how the cases fit together to conclude that  $\sigma$  is i-d on  $[-b_0, 0]$ . Further details are left to the reader.  $\square$

As this paper's grand finale, we now construct an spo for excitable dynamics on  $\mathbf{R}^2$  with the square neighborhood  $\mathcal{N}$  and threshold  $\theta = .6123$ .

*Proof of Theorem 1.5 for  $p \neq 2$ .* The first step is to verify that for the limiting dynamic with  $\theta = .6123$  there are prebugs in each direction  $\alpha$ . Combining Lemmas 6.1–6.6 we see that to produce a prebug at threshold  $\theta$  it suffices to compute five numbers and show that their minimum is at least  $\theta$ . The last five columns of Table 2 gives these five numbers for the values of  $\gamma$  considered above. To prove the existence of prebugs for intermediate values of gamma using a computer program, we need to reduce the task to a finite computation.

To do so we begin by observing that if  $D$  is the diamond with vertices  $(0, \pm\sqrt{2}), (\pm\sqrt{2}, 0)$ , and  $D'$  is  $D$  rotated by  $-\eta$ , the area of the symmetric difference of  $D$  and  $D'$  is less than four times the area of the shaded triangle in Figure 16 which is  $(1 - \cos \eta + \sin \eta)(1 + \sin \eta)$ . Now  $\sin \eta < \eta$ , and for  $\eta < 1$  we have  $\cos \eta > 1 - \eta^2/2$ , so the area in question is smaller than  $\eta + \frac{3}{2}\eta^2 + \frac{1}{2}\eta^3 \leq \eta + 2\eta^2$  when  $\eta < 1$ .

In the last paragraph we considered what happened when we changed the rectangle. As we move from one value of  $\gamma$  to another the slope changes as well. It is easy to see that, if the strip width changes by less than  $\Delta$ , the minimum strip width changes by less than  $2\sqrt{2}\Delta$ . Furthermore, if the two slopes change by less than  $\Delta$  then the other four areas of interest change by at most  $2\sqrt{2}\Delta$ . To relate these remarks to changes in the parameter  $\gamma$  we observe that for  $\gamma \in [0, 1]$ ,  $\partial w/\partial \gamma, \partial b_0/\partial \gamma$  and  $\partial b_1/\partial \gamma$  are all  $< 1$ . Investigating the values of the minimum for  $\gamma = k \cdot 10^{-5}$ , we find that in all cases the minimum of the five areas is at least .6123739 (which occurs for  $k = 84249$ ).

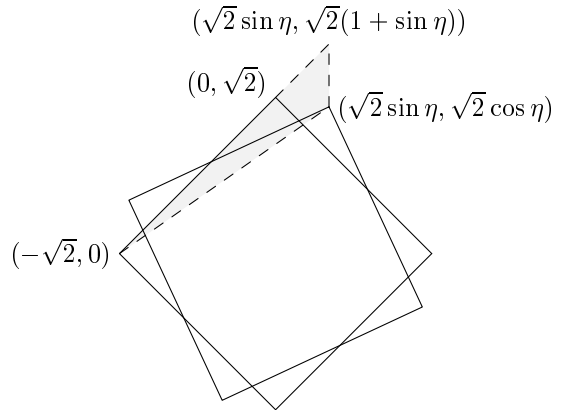


**FIGURE 16.** The area of the symmetric difference between the two squares is less than four times the area of the shaded triangle.

Since every point in  $[0, 1]$  is within  $10^{-5}/2$  of a grid point, setting  $\eta = \pi/4 \cdot 10^{-5}/2$ , it follows that at all intermediate values the minimum is larger than  $.6123739 - 4(\eta + \eta^2) - 2\sqrt{2} \cdot 10^{-5}/2 > .6123$ . The number of computations required can be reduced by a factor of 5 by noting that outside  $[.8, .9]$  the minimum is .6135, so there it suffices to investigate  $\gamma = k \cdot 10^{-4}$ .

Having produced a family of prebugs for all directions  $\alpha$ , the last step is to generalize the proof of Theorem 1.5 in the case  $p = 2$  to make an anisotropic spiral core. Let  $E_\alpha$  be our prebug of constant width  $w_\alpha$  in direction  $\alpha$ , defined on the interval  $[-l_\alpha, r_\alpha]$ . Again,  $\mathcal{R}_\alpha$  is rotation through  $\alpha$ . Write  $B_0 = E_0 + (M, 0)$ ,  $\alpha_0 = \arcsin(w_0/(M + l_0))$ , and, for  $j \geq 0$ ,

$$B_{j+1} = \mathcal{R}_{\alpha_j}(E_{\alpha_j} + (M, 0)),$$

$$\alpha_{j+1} = \alpha_j + \arcsin(w_{\alpha_j}/(M + l_{\alpha_j})).$$

Each  $\alpha_j$  is a continuous function of  $M$  and decreases to 0 as  $M \rightarrow \infty$ , so for each  $\kappa$  there is a smallest value of  $M$ , call it  $M_\kappa$ , such that  $\alpha_\kappa = 2\pi$ . Note that in this case  $B_\kappa = B_0$ .

Let  $B'_1 = B_1 \cap (E_0 + (M, w_0))$ . For  $0 < j < \kappa$ , put

$$B'_{j+1} = \mathcal{R}_{\alpha_j}(\{E_{\alpha_j} + (M, w_{\alpha_j})\}) \cap \mathcal{R}_{-\alpha_j} B_{j+1},$$

and let  $B'_0 = B'_\kappa$ . By definition  $B'_j \subset B_j$ . Write

$$\varepsilon_\kappa = \sup_{0 \leq j \leq \kappa} |B_j - B'_j|.$$

Since our prebugs vary continuously as a function of the direction  $\alpha$ ,  $\varepsilon_\kappa \rightarrow 0$  as  $\kappa \rightarrow \infty$ . It is easy to check that if  $\theta = .6123 - \varepsilon_\kappa$  and there are all 1's on  $B_j$  and 0's on  $B_{j+1}$  at time 0, then there will be all 1's on  $B_{j+1}$  at time 1. From this it follows that if we set  $\xi(x) = i$  for  $x \in B'_{\kappa-i}$ ,  $0 \leq i \leq \kappa$ , we have defined an spo for the limiting dynamic. In conclusion, we note that this construction of a core from spo's of all orientations can be applied for any value of  $p$ , proving (1.6).  $\square$

### ACKNOWLEDGMENTS

We thank our colleagues Bob Fisch, Janko Gravner, Dan Pritikin and Jeff Steif for their stimulating input as this work was taking shape. Special thanks to Janko Gravner for greatly simplifying the proof of Theorem 1.3.

Finally, we are very grateful to Silvio Levy for his extensive help with the production of the manuscript and computer graphics.

### SOFTWARE AVAILABILITY

A commented listing of the (Turbo Pascal) program `findbugs.pas` that was used to generate the data in Table 2 is available by request, as are other short programs used for various numerical calculations.

The interactive program `Excite!`, mentioned in Section 1, is also available free of charge upon request. It runs on any 80286 (or higher) PC provided with VGA (or better) graphics.

Please address requests to D. Griffeath, Mathematics Dept., University of Wisconsin, Madison WI 53706 ([griffeath@math.wisc.edu](mailto:griffeath@math.wisc.edu)).

### REFERENCES

- [Dewdney 1988] A. K. Dewdney, "Computer recreations: The hodgepodge machine makes waves", *Scientific American*, August 1988, 104–107.
- [Dewdney 1989] A. K. Dewdney, "Computer recreations: A cellular universe of debris, droplets, defects and demons", *Scientific American*, August 1989, 102–105.
- [Durrett 1991] R. Durrett, *Probability: Theory and Examples*, Wadsworth & Brooks/Cole, Pacific Grove, CA, 1991.
- [Durrett 1992] R. Durrett, "Multicolor particle systems with large threshold and range", *J. Theoretical Prob.* **4** (1992), 127–154.
- [Durrett 1993] R. Durrett, "Ten Lectures on Particle Systems", in *1993 Saint Flour Probability Summer School*, Lecture Notes in Math., Springer-Verlag, Berlin (to appear).
- [Durrett and Neuhauser 1991] R. Durrett and C. Neuhauser, "Epidemics with regrowth in  $d = 2$ ", *Ann. Appl. Probability* **1** (1991), 189–206.
- [Durrett and Steif 1991] R. Durrett and J. Steif, "Some rigorous results for the Greenberg–Hastings model", *J. Theoretical Prob.* **3** (1991), 669–690.
- [Durrett and Steif 1993] R. Durrett and J. Steif, "Fixation results for threshold voter systems", *Ann. Probability* **21** (1993), 232–247.
- [Fisch and Griffeath 1991] R. Fisch and D. Griffeath, *Excite!: a periodic wave modeling environment*. See section on software availability above.
- [Fisch et al. 1991] = [FGG] R. Fisch, J. Gravner and D. Griffeath, "Threshold-range scaling of excitable cellular automata", *Statistics and Computing* **1** (1991), 23–39.
- [Fisch et al. 1992] R. Fisch, J. Gravner and D. Griffeath, "Cyclic cellular automata in two dimensions", in *Spatial Stochastic Processes* (edited by K. Alexander and J. Watkins), Birkhäuser, Boston, 1992.
- [Fisch et al. 1993] R. Fisch, J. Gravner and D. Griffeath, "Metastability in the Greenberg–Hastings model", to appear in *Ann. Appl. Probability* **3** (1993).
- [Gerhardt et al. 1990] M. Gerhardt, H. Schuster and J. Tyson "A cellular automaton model of excitable media, II: Curvature, dispersion, rotating waves and meandering waves", *Physica D* **46** (1990), 392–415.
- [Gravner] J. Gravner, "Ring dynamics in the Greenberg–Hastings model", in preparation.

- [Gravner and Griffeath 1994] J. Gravner and D. Griffeath, "Threshold growth dynamics", to appear in *Trans. Amer. Math. Soc.* (1994).
- [Greenberg et al. 1978] J. Greenberg, B. Hassard and S. Hastings, "Pattern formation and periodic structures in systems modeled by reaction-diffusion equations", *Bull. Amer. Math. Soc.* **84** (1978), 1296–1327.
- [Greenberg and Hastings 1978] J. Greenberg and S. Hastings, "Spatial patterns for discrete models of diffusion in excitable media", *SIAM J. Appl. Math.* **34** (1978), 515–523.
- [Griffeath 1988] D. Griffeath, "Cyclic random competition: a case history in experimental mathematics", in "Computers and Mathematics", *Notices Amer. Math. Soc.* (1988), 1472–1480.
- [Kapral 1991] R. Kapral, "Discrete models for chemically reacting systems", *J. Math. Chem.* **6** (1991), 113–163.
- [Marcus et al. 1991] M. Markus, M. Krafczyk and B. Hess, "Randomized automata for isotropic modelling of two- and three-dimensional waves and spatiotemporal chaos in excitable media", in *Nonlinear Wave Processes in Excitable Media* (edited by A. Holden, M. Markus and H. Othmer), Plenum Press, New York, 1991.
- [Mikhailov 1991] A. Mikhailov, "Heart waves and the flutter that follows when they break down", *Quantum*, November/December 1991, 12–17.
- [Muller et al. 1986] S. Muller et al., "Two-dimensional spectrophotometry of spiral waves", *Physica D* **24** (1986), 71–86.
- [Newell 1983] P. C. Newell, "Attraction and adhesion in the slime mold *Dictyostelium*", pp. 43–71 in *Fungal Differentiation: A Contemporary Synthesis* (edited by J. E. Smith), Marcel Dekker, New York, 1983.
- [Toffoli and Margolus 1987] T. Toffoli and N. Margolus, *Cellular Automata Machines*, MIT Press, Cambridge, MA, 1987.
- [Weiner and Rosenblueth 1946] N. Weiner and A. Rosenblueth, "The mathematical formulation of the problem of conduction of impulses in a network of connected excitable elements, specifically in cardiac muscle", *Arch. Inst. Cardiol. Mexico* **16** (1946), 205–265.
- [Winfree 1974] A. Winfree, "Rotating chemical reactions", *Scientific American*, June 1974, 82–95.
- [Winfree 1987] A. Winfree, *When Time Breaks Down: The Three Dimensional Dynamics of Electrochemical Waves and Cardiac Arrhythmias*. Princeton Univ. Press, Princeton, NJ, 1987.

Richard Durrett, Department of Mathematics, Cornell University, Ithaca, NY 14853 (rtd@math.cornell.edu)

David Griffeath, Department of Mathematics, University of Wisconsin, Madison, WI 53706  
(griffeath@math.wisc.edu)

Received August 15, 1992; accepted July 6, 1993